

2012

3D Simulation Of Jet-A Combustion In A Model Aircraft Engine Combustion Chamber.

Mohammad Golam Mostafa
North Carolina Agricultural and Technical State University

Follow this and additional works at: <https://digital.library.ncat.edu/theses>

Recommended Citation

Mostafa, Mohammad Golam, "3D Simulation Of Jet-A Combustion In A Model Aircraft Engine Combustion Chamber." (2012). *Theses*. 90.
<https://digital.library.ncat.edu/theses/90>

This Thesis is brought to you for free and open access by the Electronic Theses and Dissertations at Aggie Digital Collections and Scholarship. It has been accepted for inclusion in Theses by an authorized administrator of Aggie Digital Collections and Scholarship. For more information, please contact iyanna@ncat.edu.

3D SIMULATION OF JET-A COMBUSTION IN A MODEL AIRCRAFT ENGINE
COMBUSTION CHAMBER

by

Mohammad Golam Mostafa

A dissertation submitted to the graduate faculty
in partial fulfillment of the requirements for the degree of
MASTER OF SCIENCE

Department: Chemical Engineering
Major: Chemical Engineering
Major Professor: Dr. Vinayak N. Kadi

North Carolina A&T State University
Greensboro, North Carolina
2012

This is to certify that the Master's Thesis of

Mohammad Golam Mostafa

has met the thesis requirement of
North Carolina Agricultural and Technical State University

Greensboro, North Carolina
2012

Approved by:

Dr. Vinayak N. Kabadi
Major Professor

Dr. Shamsuddin Ilias
Committee Member

Dr. Leonard C. Uitenham
Department Chairperson

Dr. John Kizito
Committee Member

Dr. Sanjiv Sarin
Associate Vice Chancellor for Research and Graduate Dean

Copyright by
Mohammad Golam Mostafa
2012

DEDICATION

To

*My Mother Fatema Akther
My Father Mojibur Rahman*

BIOGRAPHICAL SKETCH

Mohammad Golam Mostafa was born on October 5, 1985, in Munsiganj, Bangladesh. He received the Bachelor of Science degree in Chemical Engineering from Bangladesh University of Engineering and Technology (BUET) in March, 2009. Mr. Mostafa joined Chemical Engineering program of North Carolina A&T State University in the fall of 2010. Now he is a candidate for Master of Science in Chemical Engineering.

ACKNOWLEDGEMENTS

I convey my sincere gratitude to my advisor **Dr. Vinayak N. Kabadi**, for his continuous encouragement and guidance in advancing this research. I would also like to thank him for getting me financial support. **Special thanks to North Carolina A & T State University** for giving me the opportunity to carry out my graduate studies and conduct this little research. **Finally**, my sincere gratitude to Almighty for every of His blessings.

TABLE OF CONTENTS

LIST OF FIGURES	x
LIST OF TABLES	xiii
LIST OF SYMBOLS AND ABBREVIATION	xv
ABSTRACT	xvii
CHAPTER 1 INTRODUCTION	1
CHAPTER 2 LITERATURE REVIEW	3
2.1 Introduction	3
2.2 Background of Aircraft Engine	4
2.3. Combustion Process	6
2.4 Background of Nox Formation	12
2.5 Aircraft Engine Emission Model.....	14
2.6 Aircraft Engine Emission Assessment Procedure	15
2.7 Jet Fuel Kinetic Mechanisms	16
CHAPTER 3 CFD AND ANSYS FLUENT	21
3.1. Introduction	21
3.2 ANSYS Design Modular (DM) and Fluid Volume	22
3.3 ANSYS Meshing (AM).....	23
3.4 FLUENT Setup	27
3.4.1 Basic Fluid Flow and Balance Equations	28
3.4.2 Turbulent Chemistry Interaction.....	30

3.4.3	CHEMKIN CFD for FLUENT	33
3.4.4	Models for Turbulence.....	35
3.5	ANSYS FLUENT Solver Basics.....	36
3.6	Solution Methods	37
3.7	Solution Controls.....	38
3.8	Solution Initialization.....	38
3.9	Convergence Check and Residuals	38
CHAPTER 4 PROBLEM SET-UP AND SOLUTION		41
4.1	Introduction	41
4.2	Modeling of Combustion Chamber.....	42
4.3	Meshing.....	46
4.4	Test Matrices	50
4.4.1	Combustor Inlet Temperature and Pressure.....	52
4.4.2	Calculation of Combustor Air Flow Rate.....	54
4.5	Obtaining Boundary Conditions.....	54
4.6	Problem Set-Up.....	59
4.7	Convergence Check.....	62
CHAPTER 5 RESULTS AND DISCUSSION.....		64
5.1	Introduction	64
5.2	Comparison of NO _x Emission	64
5.3	Comparison of N ₂ O Emission	65
5.4	Comparison of CO Emission.....	66

5.5	Comparison of CH and C ₂ H ₂ Emission.....	66
5.6	Contours of Different Variables.....	68
5.6.1	Temperature Contours	69
5.6.2	Velocity Contours.....	70
5.6.3	CO Mass Fraction Contours.....	71
5.6.4	NO Mass Fraction Contours	72
5.6.5	Direction of Fluid Flow	73
5.7	Computational Expenses	74
CHAPTER 6	CONCLUSION AND RECOMMENDATIONS	76
BIBLIOGRAPHY	78
APPENDIX A	SOLVER ALGORITHMS	84
APPENDIX B	CHEMKIN FILES.....	87
APPENDIX C	MONITORING CONVERGENCE.....	92
APPENDIX D	ADDITIONAL CONTOUR PLOTS	97

LIST OF FIGURES

FIGURES	PAGE
2.1 CFM56 engine (a) Photo (b) Cross sectional diagram.....	5
2.2 Geometry of GE90 Combustion chamber.....	7
2.3 Unstructured grid of GE90 combustion chamber.....	8
2.4 Computer representation of the designed turbojet at University of Padova (a) Complete engine (b) Extended view of combustion chamber.....	10
2.5 Reference and conventional burners and their operating conditions. (a) Dimensions of different burners (b) Primary zone equivalence ratios verses overall fuel/air ratios for such burners.....	11
3.1 Steps of the integrated FLUENT solver: Geometry, Mesh, Setup, Solver and the post processor.....	22
3.2 Different types of 2D and 3D cells.....	24
4.1 Computer representation of combustion chamber geometry.....	44
4.2 Cross-section of injection system.....	45
4.3 Fluid volume considered for simulation.....	46
4.4 Meshed geometry.....	48
4.5 Skewness metrics for the generated mesh.....	49
4.6 Orthogonal quality metrics for the generated mesh.....	49
4.7 Sample rake with 6 (G1-G6) gas, 6 (P1 to P6) particle and six external (GG1 to GG6) sample probes.....	50
4.8 Workflow in FLUENT Workbench.....	61
5.1 Temperature profile. A: 7% power, B: 30% power, C: 85% power and D: 100% power settings.....	69

5.2	Velocity profile. A: 7% power, B: 30% power, C: 85% power and D: 100% power settings.....	70
5.3	CO mass fraction. A: 7% power, B: 30% power, C: 85% power and D: 100% power settings.....	71
5.4	NO mass fraction. A: 7% power, B: 30% power, C: 85% power and D: 100% power settings.....	72
5.5	Direction of fluid flow. A: 7% power, B: 30% power, C: 85% power and.....	73
A.1	Pressure Based Segregated Algorithm.....	84
A.2	Pressure Based Coupled Algorithm.....	85
A.3	Density Based Algorithm.....	86
B.1	CHEMKIN import in FLUENT Set-up.....	91
C.1	Surface monitor-average static temperatures at outlet (7% power).....	92
C.2	Surface monitor-average static temperatures at outlet (30% power).....	93
C.3	Surface monitor-average static temperatures at outlet (85% power).....	93
C.4	Surface monitor-average static temperatures at outlet (100% power).....	94
C.5	Residuals -7% power settings.....	94
C.6	Residuals -100% power settings.....	95
C.7	Residuals -85% power settings.....	95
C.8	Residuals -100% power settings.....	96
D.1	Density profile. A: 7% power, B: 30% power, C: 85% power and D: 100% power settings.....	97
D.2	Total Pressure profile. A: 7% power, B: 30% power, C: 85% power and D: 100% power settings.....	97
D.3	Contour of C ₁₂ H ₂₃ mass fraction. A: 7% power, B: 30% power, C: 85% power and D: 100% power settings.....	98
D.4	Contour of CO ₂ mass fraction. . A: 7% power, B: 30% power, C: 85% power and D: 100% power settings.....	98

D.5	Contour of N ₂ mass fraction. A: 7% power, B: 30% power, C: 85% power and D: 100% power settings.....	98
-----	---	----

LIST OF TABLES

TABLES	PAGE
3.1 Orthogonal quality and Skewness mesh metrics spectrum.....	27
4.1 Test matrices under consideration.....	51
4.2 Operating conditions for CFM-56-2C1 engine.....	52
4.3 Combustor inlet temperature and pressure.....	53
4.4 Combustor air flow rate.....	54
4.5 Primary zone equivalent ratios for different power settings.....	55
4.6 Secondary and dilution air flow distribution.....	56
4.7 Ambient conditions with engine exhaust plume temperature.....	56
4.8 Flow variables for 7% engine power setting, operating pressure 357171 Pa and inlet temperature 492.6 K.....	57
4.9 Flow variables for 30% engine power setting, operating pressure 852447 Pa and inlet temperature 635.36 K.....	57
4.10 Flow variables for 85% engine power setting, operating pressure 1850144 Pa and inlet temperature 776.55 K.....	58
4.11 Flow variables for 100% engine power setting, operating pressure 1943008 Pa and inlet temperature 784.39K.....	58
4.12 Net Mass and Heat flow rate at converged position.....	63
5.1 NO _x emission comparison for this model with APEX measured data.....	65
5.2 N ₂ O emission comparison for this model with APEX measured data.....	65
5.3 CO emission comparison for this model with APEX measured data.....	66
5.4 CH emission comparison for this model with APEX measured data.....	67

5.5 C₂H₂ emission comparison for this model with APEX measured data..... 67

LIST OF SYMBOLS AND ABBREVIATION

APEX=Aircraft Particle Emission eXperiment

AM= ANSYS Meshing

CFD=Computational Fluid Dynamics

DM=Design Modular

LTO=Landing take-off

A = an empirical constant equal to 4, Arrhenius Factor

B = an empirical constant equal to 0.5

E = Activation Energy in Arrhenius rate expression

β = Temperature exponent in Arrhenius rate expression

θ_{\max} =Largest angle in the face or cell

θ_{\min} =Smallest angle in the face or cell

θ_e = Angle for an equiangular face or cell, i.g. 60, 90 degree

$Y_{\mathfrak{R}}$ = mass fraction of any reactant, \mathfrak{R}

k = turbulent kinetic energy

ε = turbulent dissipation rate

$\nu'_{i,r}$ = stoichiometric coefficient of the reactant i in reaction r

$\nu'_{\mathfrak{R},r}$ = stoichiometric coefficient of any reactant in a reaction r

$M_{w,\mathfrak{R}}$ = molecular weight any reactant, \mathfrak{R}

$M_{w,j}$ or $M_{w,i}$ = molecular weight of species i or j respectively

$Y_{\mathfrak{R}}$ = mass fraction of any reactant, \mathfrak{R}

$\nu_{j,r}''$ = stoichiometric coefficient of the product j in reaction r

$\nu_{\mathfrak{R},r}'$ = stoichiometric coefficient of any reactant in a reaction r

ABSTRACT

Mostafa, Mohammad Golam. 3D SIMULATION OF JET-A COMBUSTION IN A MODEL AIRCRAFT ENGINE COMBUSTION CHAMBER. (**Major Professor: Dr. Vinayak N. Kabadi**), North Carolina Agricultural and Technical State University.

Aviation transportation is a major source of gaseous pollutant emissions in modern society. It is important to understand the formation, classification and mitigation of the resulting pollutants. In this work we have designed a combustion chamber to perform CFD (Computational Fluid Dynamics) simulation using ANSYS FLUENT with simplified detailed jet-A/air combustion mechanism with the purpose of predicting the major gas pollutants - mainly NO_x, CH, CO and C₂H₂. The primary objective was to compare the emission data measured on CFM56-2C1 engine during APEX (Aircraft Particle Emission eXperiment) campaign by NASA. Four engine operating conditions, idle/taxi, approach, climb and take-off have been considered. NO_x emission has been predicted in fair agreement with the APEX data. CO was highly over-predicted whereas CH and C₂H₂ were under-predicted. Several contours of different variables such as temperature, pressure, velocity, mass fraction of major species have been analyzed to understand the physics and chemistry inside the combustion chamber.

CHAPTER 1

INTRODUCTION

Aviation emissions and their impact on global climate change are becoming a great concern to scientific community and policymaker [1]. Gaseous emissions from aircraft or gas turbine engines are produced during the combustion process between fuel and air inside the engine. So, level of emission is mainly determined by the combustion process. In addition to that, pollutants coming out of such combustion processes are smaller in mass fraction than the other major combustion products such as CO₂, H₂O and N₂ etc. Because of that a successful emission modeling requires appropriate capture of the combustion process with better precision. The main step for capturing the combustion process would require a combustion kinetic scheme between the fuel and air mixture. Ideally, such combustion kinetic scheme would requires in the order of thousands species, including intermediates, or even more than that as the original fuel itself may contains several hundreds to thousands compounds [2,3]. Such a project would not be experimentally or even computationally feasible [4]. However, even though, simplification can be made in developing such scheme, question remains in solving them when coupled with CFD calculations because of limitations of current computational facilities [4].

Not only the combustion process but also the post-combustion process (turbine and nozzle) may affect pollutants formation and (or) decomposition [5]. Overall an ideal aircraft engine emission model would require a complete 3-D CFD modeling of

combustion process (fuel injection and burner) followed by the post combustion process with a comprehensive kinetic scheme. However, such modeling would require tremendous amount of computational facilities and are currently being avoided by the researchers [5,6,1,4]. Current models are either 0-D, 1-D flow calculation with detail chemistry [5] or CFD calculation with global kinetic mechanism [1] or CFD calculation with detail chemistry in reactor network model [6].

In this thesis we shall develop a 3 dimensional CFD combustion model with simplified kinetic (17 species with 26 steps) scheme to predict aircraft engine emission. Then, the model will be compared with emission data measured during APEX campaign by NASA [7]. Finally, recommendation has been made for future research directions.

CHAPTER 2

LITERATURE REVIEW

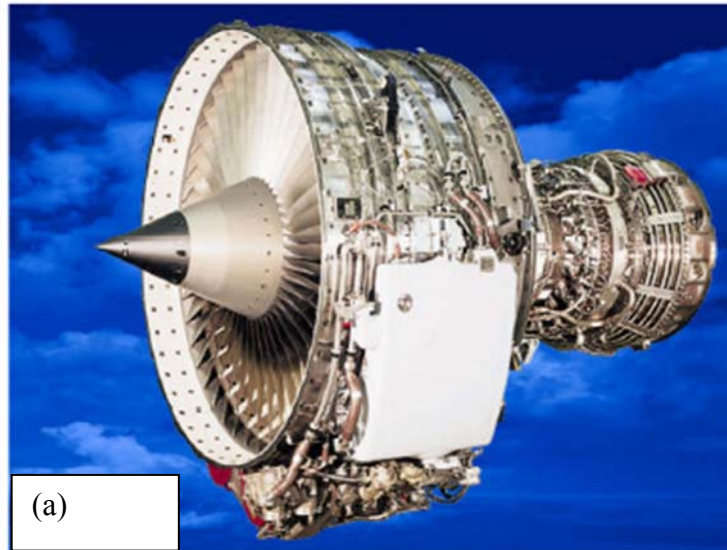
2.1 Introduction

A hypothetical perfect model for an aircraft engine emission calculation is not compatible with current computational facilities [4]. Assumptions are to be made to develop these models. However it is imperative to capture different aspects of combustion and post-combustion process with high precision to predict these low-concentration products (i. e. pollutants) in such system. Combustion process of an aircraft engine includes different burning zones called primary, secondary and dilution zone [5]. Primary burning take place right after fuel injection with swirling air that helps injection of fuel. In the primary zone burning is also called rich burning where fuel is in excess amount than the air supplied to oxidize the fuel completely. Secondary zone completes the combustion process where extra amount of air comes through some holes from the annular space. Finally dilution air is added before it goes to the turbine. These factors will be better discussed in the following sections. However, summarily, aspects of such process may include, complicated fuel injection system, primary zone fuel air ratio, secondary zone fuel air ratio, length and diameter of the combustor, operating pressure, holes distribution throughout the chamber, diameters of these holes and total pressure at the annular space from where secondary and dilution air flow to the chamber. Proper modeling for emission prediction of such system requires proper mimicry of all these variables. In this chapter several facts will be presented that dictate aircraft engine emissions and the

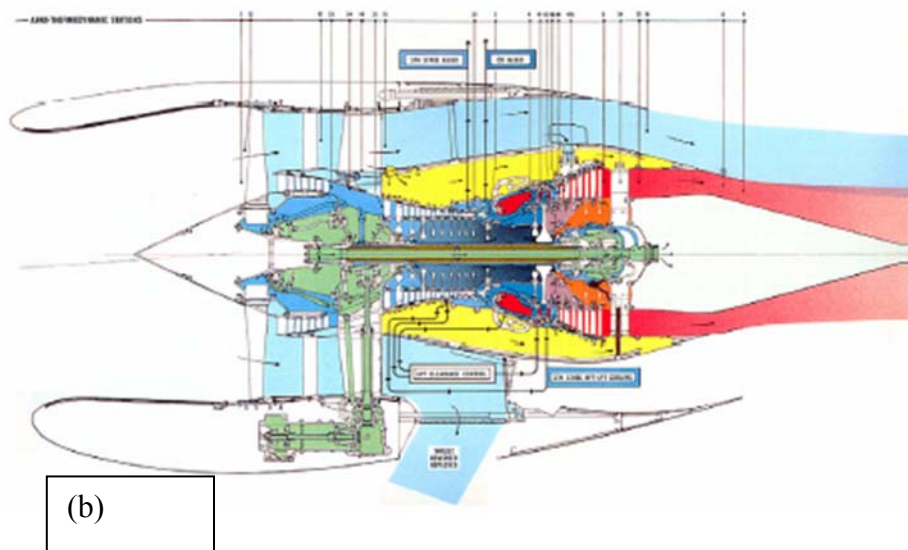
important factors to consider in the modeling process. Primarily such factors may include geometry and size of the combustion chamber, kinetic mechanism of combustion process and modeling scheme (i.e. 3-D CFD, 0-D gas parcel, CFD with reactor network).

2.2 Background of Aircraft Engine

An aircraft engine consists of four different major components: compressor, combustor, and turbine and exhaust system. Figure 2.1 [7] shows a schematic for 'CFM56' engine. The first step is to compress the atmospheric air to a high pressure. The compression system many consists of several stages. Usually the first stage is of compression, in turbo fan engine, is done using large diameter propeller. After first stage compression using diameter large fan/propeller (figure 2.1(a) -in the left), some of the air goes into low pressure and subsequently high pressure compressor, another big portion of the air called bypass air, does not take part into further pressure increase or in combustion rather directly mixes with turbine exhaust and mainly responsible for increasing engine thrust and lowering pollutant concentration in the exhaust. In figure 2.1 this bypass air is shown by bright green color. The ratio of the air flowing outside of low and high pressure compressor to the air flowing through them is called bypass ratio. Then the compressed air from high pressure compressor directly goes into combustor. The combustion process increases the fluid temperature up-to 1000°C-1700°C depending on the engine power requirement [8]. After that the accumulated energy is extracted in the turbine section. The power produces by turbine mainly runs the compressor system of the engine by a concentric shaft and produces little electric power.



(a)



(b)

Figure 2.1 CFM56 engine (a) Photo (b) Cross sectional diagram.

After power extraction by the turbine the fluid mixture goes into the exhaust assembly and to the atmosphere subsequently. This exhaust gas produces thrust according to the Newton's second law of motion and which is responsible to move the aircraft forward. However thrust produced by the engine can vary depending on the engine operating

condition and by its type. The following engine characteristics has been found for CFM56-2C1 engine in the engine manufacture data sheet [8].

Maximum takeoff thrust (lb)	22,000
Maximum Climb Thrust (lb)	5,400
Maximum cruise thrust (lb)	4,980
Overall pressure ratio at maximum climb	31.3
Bypass Ratio	6.0
Length (in)	95.7
Fan diameter (in)	68.3
Basic dry weight (lb)	4,635

However based on scope of this thesis we shall limit our discussion on combustion process only.

2.3. Combustion Process

A combustor is consists of a complicated fuel injection system and burning zone. The burning zone can be divided into several sub-zones such as, primary burning zone, secondary burning zone and dilution zone. After initial injection of fuel with some air, additional air also added through some holes along the length of the combustion chamber [9]. The primary reasons for adding air through the holes are to control the combustion process in terms of equivalence ratios, create turbulence to facilitate combustion process and to protect the combustion liner and turbine blade from high temperature mechanical

failure. Figure 2.2 shows a computer representation of a ‘GE90’ combustion chamber [10].

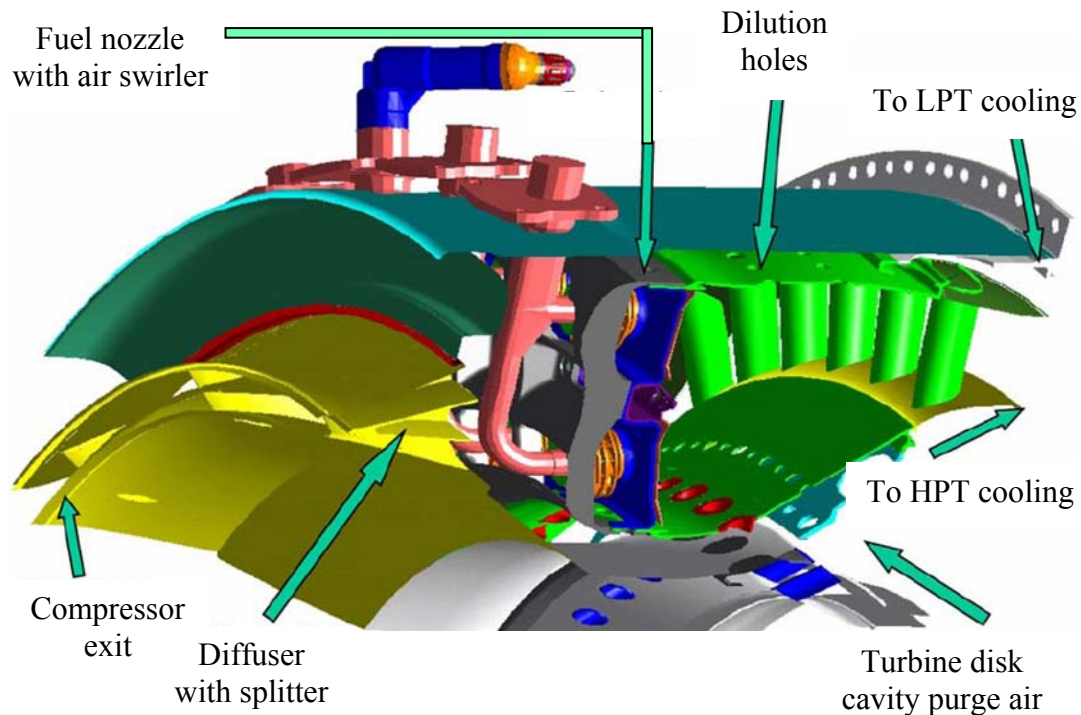


Figure 2.2 Geometry of GE90 Combustion chamber.

In this figure the dual annular fuel nozzle arrangement with air swirler can be seen. High pressure turbine (HPT) nozzle is also detectable. At the inlet of the combustion chamber diffuser has been attached to lower the fluid velocity before it goes to combustion chamber. Although figure 2.2 gives a general overview of aircraft engine combustion chamber, no information has been provided about the length and diameters of the combustion chamber by Turner et al [10]. NASA has done a high-fidelity three dimensional CFD simulation for the GE90 engine including combustion chamber [10]. One of the objectives was to show the CPU time required to perform these simulations

for a supercomputing facility. It took over 5hr to run the simulation. The number of processors used was different for different sections. Simulation of high pressure compressor has done using 512 processors in nearly 2hr. Turbine section took nearly 2hr with 512 processors. Figure 2.3 [10] shows a meshed (i.e. divided into finite elements) combustion chamber that can be used for CFD analysis. The gridded combustor had 1.1 million tetrahedron cells and its simulation took nearly 12 min with 256 processors. However the number of species used in that simulation was unknown. The simulation also reproduced the major variables such as total pressure, total temperature and flow rate over the whole engine.

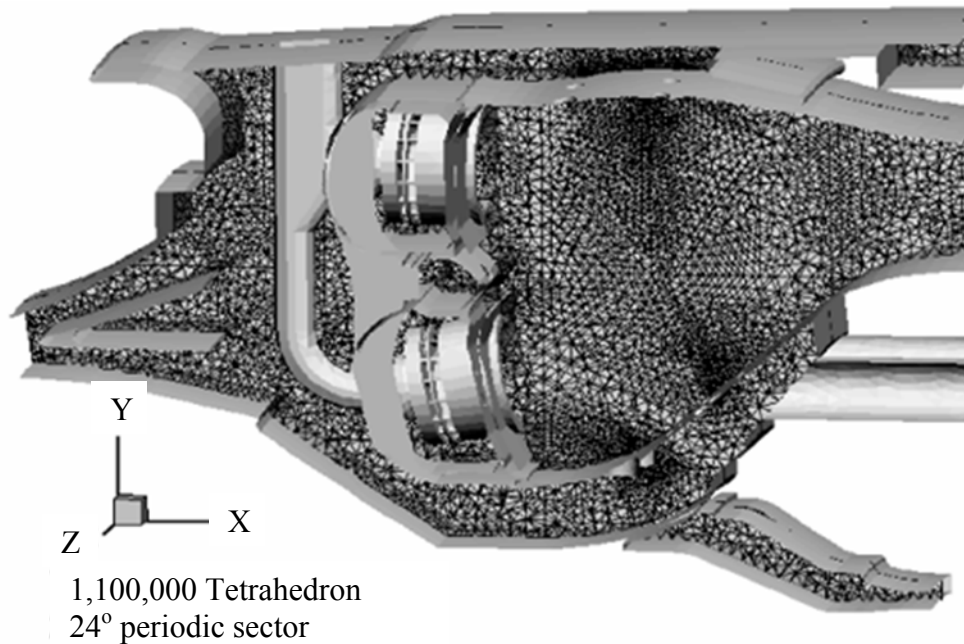


Figure 2.3 Unstructured grid of GE90 combustion chamber.

Figure 2.4 shows a laboratory scale jet engine produced by Benini and Giacometti at University of Padova [11]. In figure 2.4 (a) different sections - compressor, combustor and turbine of this engine have been shown. The engine has $377\text{N}/(\text{kg}/\text{s})$ maximum specific thrust and 2.66 maximum pressure ratio. They explained detail development of all the phases from design, manufacturing and operation. Figure 2.4 (b) shows an extended view of combustion chamber. Although engine uses an annular combustion chamber working principle is different from an actual jet engine combustion chamber. The air and fuel come from a different direction and maintain proper mixing and residence time in the chamber. As it is a small scale jet engine it was challenging to maintain the combustion chamber residence time in such a short length. And thus circular flow path has been adopted to overcome this fact. Main reason for building such engine was for didactic and research activities. Benini et al [1] have performed a NO_x emission study on their designed combustion chamber by both experimentally and CFD simulation and demonstrated that NO_x emission can be reduced by direct water steam injection. In their study for a certain optimal condition, NO_x emission was nearly 13.82g per kg fuel burnt. Another type of combustor is called Conventional Baseline Burners. These types of combustor are also called can combustor. Figure 2.5 (a) shows schematic of conventional burner and reference burner [9]. The length and combustor centerline distance from axis of engine is also shown also shown in the figure 2.5 (a). If the chambers were drawn by scale the diameters of V2500 engines seem half of its length, 8in.

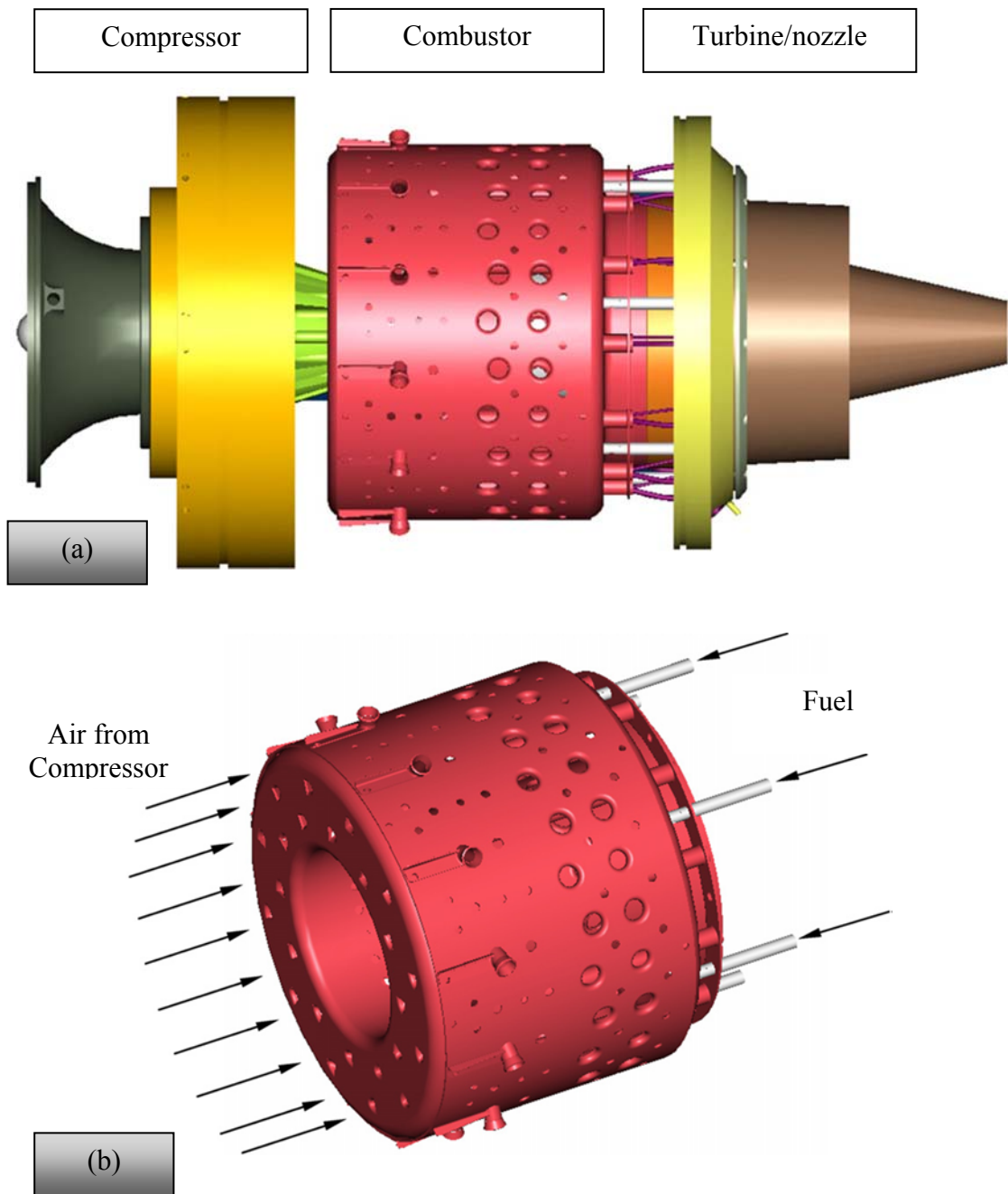


Figure 2.4 Computer representation of the designed turbojet at University of Padova (a) Complete engine (b) Extended view of combustion chamber.

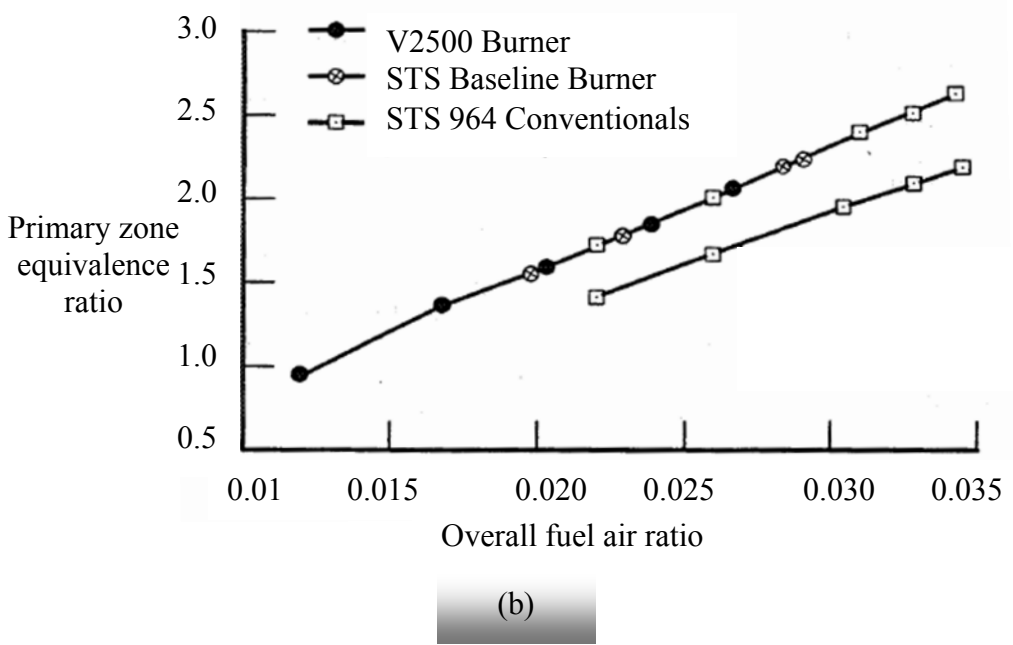
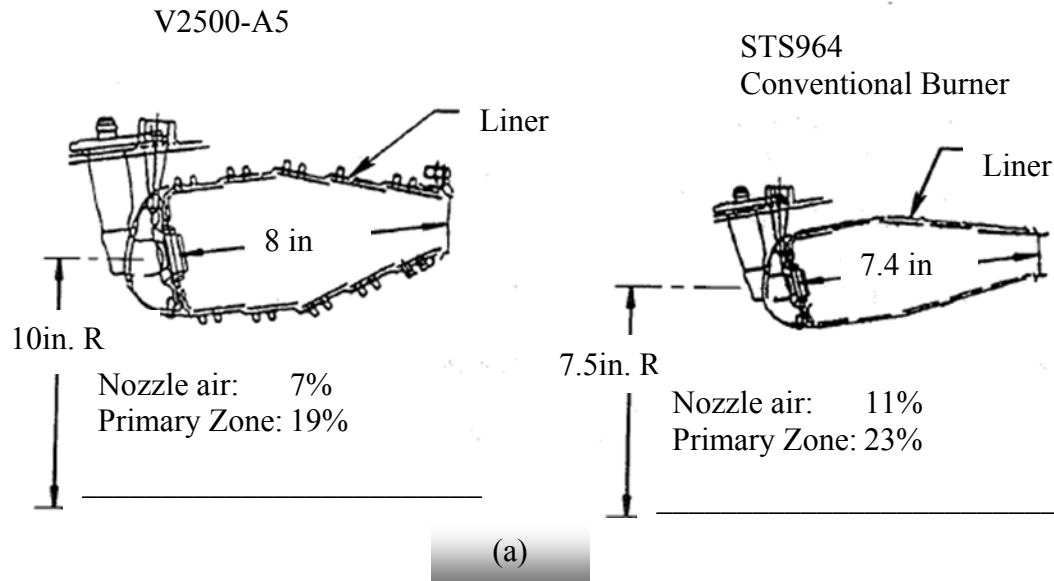


Figure 2.5 Reference and conventional burners and their operating conditions. (a) Dimensions of different burners (b) Primary zone equivalence ratios verses overall fuel/air ratios for such burners.

From simple trigonometry it can be found that the engine can accommodate as much as 15.7 combustion chambers. However additional space must require if each chamber needs a casing from where dilution air must flow to the chamber. Some operating conditions for such as engine is also depicted in the figure 2.5. For V2500-A5 the primary zone air flows is 19% of the total air flow where as for STS964 this value 23%. Figures 2.5 (b) shows primary zone equivalence ratios relative to engine overall fuel air ratios [9].

Although discrete information are available about the geometry of and some aspects of combustion chamber in different open literatures [9,11], no specific details has been included in any one of those literatures about their dimensions and detail design on a specific engine. The logical explanation is these are proprietary information of engine manufacture and are not open to public. However individual or academic researchers probably are badly in need of that information to check the consistencies of different cases.

2.4 Background of Nox Formation

Nitrogen oxides (NO_x) form when fuel is burned at high temperatures, as in a combustion process. The most important sources of NO_x are motor vehicles, electric utilities, and other industrial, commercial, and residential sources that burn fuels. Nitrogen oxides (NO_x), is the generic term for a group of highly reactive gases, all of which contain nitrogen and oxygen in varying amounts. Most of the nitrogen oxides are colorless and odorless. However, one common pollutant, nitrogen dioxide (NO₂) along

with particles in the air can often be seen as a reddish-brown layer over many urban areas. NO_x is responsible for smog, acid rain, global warming and many other health and environmental impacts [12].

In engine exhaust, NO_x is mainly composed of NO, with smaller amounts of NO₂ [13,14]. Most of time, other oxides of nitrogen-such as N₂O, N₂O₅ and NO₃ are negligible. However three process described below are believed to be important in the formation of NO_x [13].

Thermal NO_x:

Thermal NO_x are the products of reaction between N₂ and O₂ at high temperature. Usually N₂ and O₂ react through a series of chemical steps and produces different nitrogen oxides. These NO_x are called thermal NO_x depending on the production process. Thermal NO_x formation occurs at temperatures above 1500 °C, and the rate of formation increases rapidly with increasing temperature [13]. Generally thermal NO_x production rate are independent of fuel chemistry.

Prompt NO_x:

When large or small hydrocarbons get involved into combustion process, usually they break down to smaller intermediates such as CH or CH₂. In the process these intermediates may reacts to form different CN compounds. Subsequent oxidation of these CN compounds many produces different nitrogen oxides. This process of NO_x production is called prompt NO_x [13,14]. Prompt NO_x is highly dependent on fuel chemistry. If there are lots of hydrocarbon fragments, especially in the fuel rich condition, prevalence of prompt NO_x can be observed.

Fuel NOx:

If fuel itself contains nitrogen and subsequent oxidation of that fuel may produce NO_x are called fuel NO_x. However generally nitrogen level in fuel is extremely low and NO_x from this formation process is low.

2.5 Aircraft Engine Emission Model

Literature review shows that pollution calculation model for aircraft engine are extremely sparse. Major pollutants for aircraft engine are CO, NO_x, HC, and smoke number. Smith [9] has presented some emission models for advanced subsonic combustion chamber. They also showed that NO_x emission varies depending on combustor and engine operating conditions. And NO_x emission index ranges from 3gm per kg fuel to 33gm per kg fuel burnt. These models are based on pressure, temperature, humidity and different empirical coefficients. They also tabulated the emission data for different operating conditions for different types of burner. Among the rigorous modeling Fichet et al [6] have presented a reactor network model for predicting NO_x emission in gas turbine engine using detail chemistry. In that work they split the CFD computed flow field into several homogenous zones considered as perfectly stirred reactor where detail chemistry can be included without flow calculation. This partially coupled CFD and details kinetics modeling helps to avoid excessive CPU requirements. Moniruzzaman et al [5] have developed a zero dimensional aircraft engine emission mode using detail chemistry. This model is based on gas parcel model. This can also be called series of perfectly mixed gas reactor and thus reactor network. They predicted several major and minor pollutants

species and compared with APEX measured data. Benini et al [1] have done a CFD simulation on the combustion chamber built at University of Padova. However the simulation was based on simple chemistry. They demonstrated that NO formation can be reduced by direct water/steam injection. Wey et al [7] presented a extensive experimentally measured pollutants data including NO_x, SO_x, HC etc. obtained from APEX (Aircraft Particle Emission eXperiment) campaign.

Several models to predict NO_x formation in diesel engine are currently being explored. [15,16]. Aithal [17] has developed a model based on finite rate chemistry. Khoshhal et al [18] have done a sensitivity analysis for fuel temperature on NO_x formation in a furnace. Among the reduction techniques catalytic reduction [19] and steam/water injection [1] are suggested by the researchers.

2.6 Aircraft Engine Emission Assessment Procedure

Emission Assessment is a way of expressing pollutants level that emits from aircraft engine. Two types of emission estimating procedures are described in Smith [9]. One, every emission level can be described as g (gram) of pollutants per kg (kilogram) fuel burned. Another way is based on landing/take off (LTO) cycle. The main objective of this type of measurement is to simulate aircraft operation in the vicinity of an airport. This LTO cycle includes four steps

1. Takeoff , associated with 100% rated thrust for 0.7 minutes
2. Climb, associated with 85% thrust for 2.2 minutes
3. Approach, associated with 30% thrust for 4.0 minutes

4. Taxi/idle, associated with 7% thrust for 26.0 minutes

These four steps are also called ICAO (International Civil Aviation Organization) based LTO cycle. Total mass of the pollutants are individually summed during this four phases and then this summation is normalized by 100% rated thrust to produce a characteristics number called EPAP (Environmental Protection Agency Parameter). The unit of EPAP is gram-pollutants per kN maximum rated thrust. Other than these methods Mazaheri et al [20] have defined different emission assessment procedure and provided an inventory of gaseous emission from a large aircraft. Kurniawan et al [21] present a comparison of different assessing techniques. They showed that different assessing methods cause a variation in results of pollutant emission in LTO cycle.

2.7 Jet Fuel Kinetic Mechanisms

Jet fuel combustion kinetics is extremely important in order to develop a model that will predict emission from jet engine. Without proper kinetics all the attempts will go in vain. Although kinetics of jet fuel are still under-developed, significant progress has been made in this area in the recent decades. Development of detailed chemical kinetic models is extremely challenging. Gasoline, diesel and jet fuels derived from different sources are composed of hundreds to thousands of compounds [22]. However detailed kinetic models for such fuels cannot contain all the compounds due to the limitation of current computational resources [22,4,23]. Because of that a simplified mixture called surrogate mixture must be defined before attempting to develop a kinetic model. Sometimes the fact of limited computational resources can be addressed by reducing detailed kinetics by

some optimization techniques [24,4,23,25,26]. Jet fuels are kerosene-type cut of petroleum containing C-10 to C-18 hydrocarbons, including alkanes, cycloalkanes and aromatic compounds. The criteria and process of developing a surrogate mixture are not unique. However a proper surrogate fuel must have equivalent physical and chemical properties as the fuel it is representing. Violi et al [27] developed a JP-8 surrogate based on the following criteria:

1. It was assumed that chemical kinetics for each candidate fuel is known.
2. Simplicity must be maintained due to limited computational capabilities.
3. The surrogate is required to match practical fuels in both physical and chemical properties: (a) volatility - boiling range and flash point; (b) sooting tendency - smoking point and luminous number; (c) combustion property - heat of combustion, flammability, and reaction rates.

Based on these criteria they developed three surrogate mixtures for JP-8 fuels. The most extensive one has 15% m-Xylene, 10% isooctane, 20% methylcyclohexane, 30% dodecane, 20% tetradecane, 5% tetralin by volume. Humer et al [28] proposed three components surrogate model for jet fuels based on 60 % n-alkanes, 20 % cycloalkanes and 20% aromatics. Aksit and Moss [29] have developed a simple surrogate mixture to reproduce the sooting behavior of aviation kerosene. Their surrogate mixture includes 20% propyl benzene and 80% n-decane by mass. Dagaut et al [3] have developed 1 to 3 component surrogate fuel in order to reproduce kinetics for kerosene combustion. Wang [30] has developed one component ($C_{12}H_{24}$) surrogate fuel based on thermophysical characterization of kerosene combustion. It is also observed that, in addition to separate

effort to model a surrogate mixture all the kinetics modeling for a specific named fuel (jet, diesel fuel) starts by defining a surrogate mixture first [31,32,33]. Dagaut et al [34] have done an extensive literature survey for the chemical kinetics of combustion of jet fuel. For kinetic model development, general procedures require data such as concentration profile versus time, concentration profile versus temperature, concentration profile versus distance to the burner. [35,36,37,38]

Gueret et al [31] developed a kinetic scheme based on 3 components (79% undecane, 10% n-propylcyclo-hexane and 11% 1,2,4 trimethylbenzene by weight) surrogate mixture. In this scheme quasi-global expressions are given for larger hydrocarbon cracking (partial oxidation). For the smaller hydrocarbon (up to C₄ compounds) a reduced detail mechanism has been proposed with 56 species and 360 reactions with their reverse reactions. Concentration profiles versus time were modeled and major species were simulated correctly. Cathonnet et al. [35] modeled kerosene kinetics in a jet stirred reactor (JSR) using model fuel: n-decane with 603 reversible reactions and 78 species. Concentration profiles and time were correlated consistently. Dagaut et al. [36,37] used n-decane as a surrogate fuel and kinetic modeling has been done using 573 reversible reactions and 90 species. Riesmeier et al. [39] have done flamelet modeling including NO_x and soot formation using n-decane and 1,2,4-trimethylbenzene as surrogate mixture. The model of Cathonnet et al. [38] incorporates 1463 reversible reactions and 188 species. Their surrogate mixture includes species 78% n-decane, 9.8% cyclohexane, 12.2% toluene (by volume). Dagaut [40] kerosene kinetics include 1592 reversible reactions, 207 species with 74% n-decane, 11% n-propylcyclohexane, 15% n-

propylbenzene (by volume) surrogate mixture. Wen et al. [41] modeled soot volume fraction, temperature, mixture fraction using 1592 reversible reactions and 207 species. Dagaut et al [42] studied the chemical kinetics for jet fuel with bio-fuel additives and developed a scheme with 2027 reversible reaction and 263 species.

Although literature reviews show that there are enough kinetic models available for jet fuel combustion, only few are suitable to satisfy our current needs. Based on our objective to predict aircraft engine emission specifically NO_x using CFD software packages we needed a jet fuel kinetic mechanism that will fairly predict NO_x formation in an aircraft engine. As CFD with finite rate chemistry is computationally highly expensive and stiff, number of species in the kinetic scheme needs to be limited. Kundu et al [14] have provided a kinetic scheme with NO_x chemistry based on 17 species and 26 step reaction for jet-A. The mechanism has been developed specifically to predict NO_x formation during combustion of aviation kerosene. However the mechanism does not cover the entire range of operating conditions for actual aircraft engine. To limit the number of species the mechanism does not include NO₂. Arrhenius coefficients have been given only for 5atm pressure. Pressure dependencies must be accounted for to generalize the mechanism. Wang [30] has proposed kinetic scheme for aviation kerosene based on 10 species. The purpose of this scheme is to predict soot formation in CFD computation. Although major pollutants from an aircraft are CO, unburned HC, NO_x and soot particles, trade-off exists between those pollutants. For example if the designer wants to reduce the NO_x by lowering the residence time of the fuel and air mixture in the burner he has to be ready to accept more pollution in terms of unburned HC and (or) soot level.

Based on this fact a single mechanism with fewer species (i.e. 10 to 25 species) needs to be considered in order to understand emission phenomena or to optimize the level of different pollutants simultaneously. But no such mechanism with 10 to 25 species could be found in the current literature that would facilitate CFD study for proper emission prediction. Thus current emission models are avoiding direct CFD or accepting it partially [6].

Extensively developed CH₄ based NO_x and SO_x detail chemistry is available at University of Leeds website [43]. NO_x and JP-10 Chemistry are available at University of California San Diego website [44]. However these NO_x chemistries are based on low hydrocarbon such as CH₄, and thus, to use them for jet fuel combustion, one must assume that there are no significant NO_x formation reactions between higher hydrocarbon and different N or O pathways. Even with this limitation when NO_x and actual fuel chemistry are merged they may end up with several hundred species. Hoekman et al [13] studied NO_x emissions for biodiesel and found increased NO_x with biodiesel. That clearly suggests that NO_x chemistry must be developed together with fuel chemistry. And thus realistic chemistry gets even more complicated. Lu and Law [4] have also explained the importance of comprehensiveness of detailed chemistry. However accommodating realistic fuel chemistry with current computational capabilities is quite difficult [4]. Based on these facts it suggests that detail chemistry has a restricted use in CFD. As a mitigative measure researchers have put their emphasis on finding optimization techniques for mechanism reduction [4,23,25,26].

CHAPTER 3

CFD AND ANSYS FLUENT

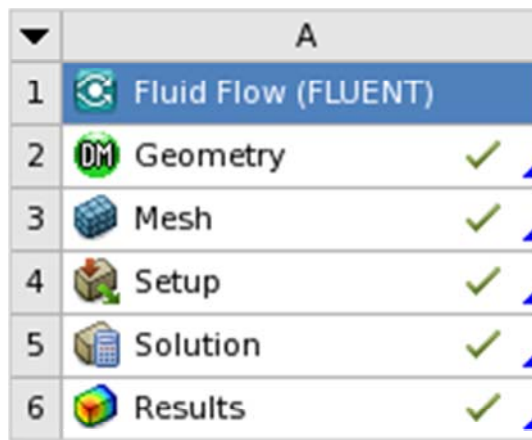
3.1. Introduction

With growing computational facilities CFD became a cynosure of many researchers and industrial personnel. Due to their increased demand several commercial CFD solver packages are also available nowadays. ANSYS, Inc. [45] has two different solvers i.e. FLUENT and CFX. Both of the solvers come as integrated packages with geometry modeling, grid generation and post-processing. FLUENT is seen as a more general code while CFX has traditionally been focused on turbo-machinery applications. CD-Adapco. [46] offers STAR-CCM+ and STAR-CD. STAR-CCM+ is a highly comprehensive solver that can include problems involving multi-physics and complex geometries on the other hand STAR-CD is mainly for internal combustion engine simulations. Aerosoft, Inc. [47] provides GASP solver which primarily facilitates aerodynamic design. Other than these, COBALT code from Cobalt Solutions, LLC. [48] and CFD++ from Metacomp Technologies, Inc. [49] can be considered as major commercial CFD solvers, by reputation. NASA Glenn Research Center has also developed APNASA, a turbo-machinery flow code, and National Combustor Code (NCC) which is primarily for jet engine combustor simulation. As our current work has been done by FLUENT, rest of the sections of this chapter will elaborate different aspects of FLUENT in relation to this work. FLUENT is an integrated software package that allows to create geometry which is consistent with control volume of fluid to be simulated, generate mesh, set up boundary

conditions and solve the problem. It has also a post-processor that allows reporting and visualization of results.

3.2 ANSYS Design Modular (DM) and Fluid Volume

The first step for solving a CFD problem is to define the boundary of fluid volume which is to be simulated. FLUENT provides a feature called Design Modular (DM) which is one the preprocessor of main solver. The figure 3.1 shows different steps of FLUENT solver package. The first step is to create geometry and after geometry creation the geometry can be transferred to ‘Mesh’ and geometry can be gridded by that module. After meshing the geometry it is necessary to load the gridded geometry into ‘Setup’.



	A
1	Fluid Flow (FLUENT)
2	Geometry ✓
3	Mesh ✓
4	Setup ✓
5	Solution ✓
6	Results ✓

Figure 3.1 Steps of the integrated FLUENT solver: Geometry, Mesh, Setup, Solver and the post processor.

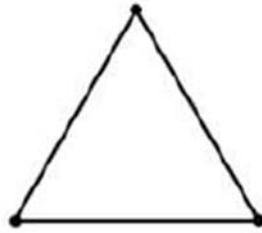
In the ‘Setup’ user will be able to define boundary conditions and make it ready to send it to the actual fluent solver (‘Solution’). Finally solutions can be visualized and other operations can be done using the fluent post-processor (‘Results’).

The purpose DM is to create a 2D/3D geometry of the fluid. 3D geometries are created from 2D sketches by some operation i.e. ‘Extrude’, ‘Revolve’, etc. This DM can also be used to import a dirty CAD geometry and perform various operations to prepare it for meshing. It also allows certain dimension parameterization which is indispensable if user wants to optimize certain geometry. In this work we have used DM to build the fluid-geometry. The necessary steps and details of geometry creation will be discussed in the next chapter.

3.3 ANSYS Meshing (AM)

The second pre-processor of the FLUENT is ANSYS Meshing. The purpose of the ANSYS Meshing is to mesh the fluid volume in an efficient way so that solver can produce a converged results in a comparable less amount of time. There are six meshing method in the ANSYS Meshing (version 13) for 3-D geometries, which are Tetrahedrons, Sweep, MultiZone, Hex Dominant, Automatic and Cutcell [50]. Figure 3.2 gives an overview of different types of elements. For 2D geometries it can generate triangular cells, quadrilateral cells or a mixture of quadrilateral and triangular cells.

2D Cell Types

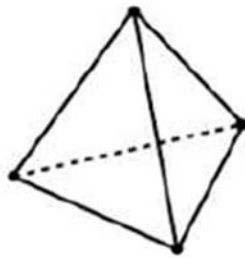


Triangle

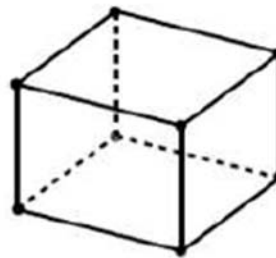


Quadrilateral

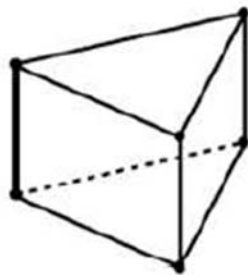
3D Cell Types



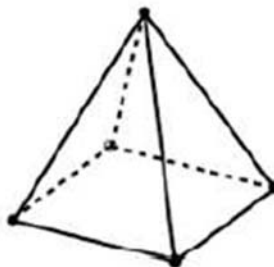
Tetrahedron



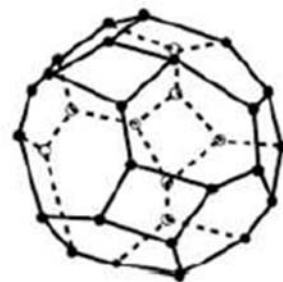
Hexahedron



Prism/Wedge



Pyramid



Polyhedron

Figure 3.2 Different types of 2D and 3D cells.

As the name suggests Tetrahedrons method produces tetrahedron elements. Sweeps generates prisms or hexahedral elements. MultiZone and Hex Dominant method produce mainly hexahedral with some other types of elements. Automatic method is an integrated method that combines multiple methods based on complexity of the geometry and produces a relatively better mesh, not necessarily all the time. Cutcell method generates cells by cutting the fluid volume directly in a Cartesian coordinate and this method mainly produces hexahedral elements.

Other features of ANSYS Meshing include ‘Inflation’, ‘Match control’, ‘Global Mesh Control’ and different size control tools etc. The purpose of ‘inflation’ is to add extra elements near wall so that solver can properly capture the aspects of boundary layer. ‘Match control’ matches the mesh on two faces or two edges on a body element. Matching of mesh on two faces is important for problem involving periodic boundary conditions. As periodic boundaries are supposed to have same solutions it is necessary to replicate the faces in mesh also. And FLUENT won’t allow setting the faces periodic unless the faces match each other. ‘Global mesh control’ is a graphical user interface (GUI) that allows controlling minimum and maximum cell-size, meshing algorithm and to check mesh-qualities.

Mesh quality control is an important aspect in CFD simulation. ANSYS Meshing provide several mesh quality measurement tools such as orthogonal quality, skewness, maximum corner angle, wrapping factor, Jacobian ratios, aspect ratios etc. However actual mesh quality can be determined from the values of orthogonal quality, skewness metrics.

Skewness:

Skewness is one the primary quality measures for a mesh [50]. Skewness determines how close to ideal (equilateral or equiangular) a face or cell is. In the equilateral volume based deviation method, skewness is defined as

$$\text{Skewness} = \frac{\text{Optimum Cell Size} - \text{Cell Size}}{\text{Cell Size}} \quad 3.1$$

Skewness can be also defined by normalized angle deviation method and mathematically,

$$\text{Skewness} = \max \left[\frac{\theta_{\max} - \theta_e}{180 - \theta_e}, \frac{\theta_e - \theta_{\min}}{\theta_e} \right] \quad 3.2$$

Where,

θ_{\max} = Largest angle in the face or cell

θ_{\min} = Smallest angle in the face or cell

θ_e = Angle for an equiangular face or cell, i.g. 60, 90 degree

In which it suggests how the angle of the element faces are deviated from a ideal equiangular element.

Orthogonal quality:

Orthogonal quality is another major quality measure for a mesh. Orthogonal quality for a cell is computed as minimum of the following quantities computed for each face i :

$$\frac{\bar{A}_i \cdot \bar{f}_i}{|\bar{A}_i| |\bar{f}_i|} \quad \text{and} \quad \frac{\bar{A}_i \cdot \bar{c}_i}{|\bar{A}_i| |\bar{c}_i|}$$

where,

\bar{A}_i is the face normal vector

\bar{f}_i is a vector from the centroid of the cell to the centroid of that face

\vec{c}_i is a vector from the centroid of the cell to the centroid of the adjacent cell that share the face.

Low orthogonal quality or high skewness values are not recommended. Ansys, Inc. recommends to consider table 3.1 as general guideline [50].

Table 3.1 Orthogonal quality and Skewness mesh metrics spectrum.

Recommendation	Orthogonal Quality	Skewness
Excellent	0.95-1.00	0-0.25
Very Good	0.70-0.95	0.25-0.50
Good	0.20-0.69	0.50-0.80
Acceptable	0.10-0.20	0.80-0.94
Bad	0.001-0.10	0.95-0.97
Inacceptable	0-0.001	0.98-1.00

3.4 FLUENT Setup

The next important step of the simulation is to prepare the solver to start calculation and the step is called ‘Setup’. This step is also called FLUENT Solver pre-processor. In relation to this thesis few aspects of ‘Setup’ will be elaborated and different options will be explored.

3.4.1 Basic Fluid Flow and Balance Equations

ANSYS fluent provides comprehensive modeling capabilities. Modeling can be done with any combination of the followings but not limited to-

- ✓ Steady state flow / transient flow
- ✓ Compressible / incompressible flow,
- ✓ Laminar flow / turbulent flow
- ✓ Multiphase flow
- ✓ Discrete phase modeling
- ✓ Chemical reaction (Volumetric, Surface or Chemical Vapor Deposition)
- ✓ Heat exchanger modeling
- ✓ Porous media modeling

However in this thesis steady, compressible turbulent flow with volumetric reactions has been considered and these phenomena are discussed. For all types of modeling ANSYS FLUENT solves conservation equation for mass and momentum (Equation. 3.3 and 3.4 respectively). As our system includes reactions it must include energy balance equation (Equation 3.6) and species conservation equation (Equation 3.10). A Major limitation of ANSYS FLUENT is that it cannot handle more than 50 species [51]. However, that number (i.e. 50 species) is probably high enough to slow down a super computer considerably.

Conservation of Mass equation:

$$\frac{\partial \rho}{\partial t} + \nabla \cdot (\rho \vec{v}) = S_m \quad 3.3$$

S_m is the mass added to the continuous phase from a dispersed second phase (i.e. due to vaporization of liquid droplets or any user defined source terms)

Conservation of Momentum Equation:

$$\frac{\partial}{\partial t}(\rho \vec{v}) + \nabla \cdot (\rho \vec{v} \vec{v}) = -\nabla p + \nabla \cdot (\overline{\overline{\tau}}) + \rho \vec{g} + \overline{F} \quad 3.4$$

Where p is the static pressure, $\overline{\overline{\tau}}$ is the stress tensor, $\rho \vec{g}$ and \overline{F} are the gravitational body force and external body forces respectively. The stress tensor $\overline{\overline{\tau}}$ is given by

$$\overline{\overline{\tau}} = \mu \left[\left(\nabla \vec{v} + \nabla \nabla \vec{v}^T \right) - \frac{2}{3} \nabla \cdot \vec{v} I \right] \quad 3.5$$

Where, μ is molecular viscosity I is the unit tensor.

Energy Conservation Equation:

$$\frac{\partial}{\partial t}(\rho E) + \nabla \cdot (\vec{v}(\rho E + p)) = \nabla \cdot \left(k_{eff} \nabla T - \sum_j h_j \overline{J}_j + (\overline{\overline{\tau}}_{eff} \cdot \vec{v}) \right) + S_h \quad 3.6$$

Where, k_{eff} is the effective conductivity, $(k+k_t)$ and k_t turbulence thermal conductivity,

\overline{J}_j is the diffusion flux of species j , S_h includes heat of chemical reactions and other user

defined heat sources. E of can be breakdown as equation 3.7

$$E = h - \frac{p}{\rho} + \frac{v^2}{2} \quad 3.7$$

where sensible enthalpy (h) can be defined by equation 3.8

$$h = \sum_j Y_j h_j + \frac{p}{\rho} \quad 3.8$$

$$\text{where, } h_j = \int_{T_{ref}}^T C_{p,j} dt \quad 3.9$$

Species Transport Equation:

$$\frac{\partial}{\partial t}(\rho Y_i) + \nabla \cdot (\rho \bar{v} Y_i) = -\nabla \cdot \bar{J}_i + R_i + S_i \quad 3.10$$

Where R_i net rate production of species due to chemical reaction and S_i net rate of other source term. ANSYS FLUENT models mass diffusion \bar{J}_i in turbulent flows by the equation 3.11

$$\bar{J}_i = -\left(\rho D_{i,m} + \frac{\mu_t}{Sc_t}\right) \nabla Y_i - D_{T,i} \frac{\nabla T}{T} \quad 3.11$$

Sc_t is the turbulent Schmidt number, $\frac{\mu_t}{\rho D_t}$ and D_t is turbulent diffusivity. Turbulent diffusivity generally overwhelms the laminar diffusivity.

3.4.2 Turbulent Chemistry Interaction

In an actual turbulent flow how the finite rate chemistry is modeled will be discussed here. ANSYS FLUENT provides three different ways to integrate finite rate chemistry into turbulent flows.

Laminar Finite Rate:

In this model reaction rates determined by the Arrhenius kinetic expression and effects of turbulent fluctuation are ignored. This model is exact for laminar flow but it produces inaccurate results for turbulent flows. However this laminar rate modeling may be acceptable in some cases where the chemistry is very slow or slow turbulent-chemistry

interaction such as supersonic flames. This model is computationally cheaper than EDC (Eddy Dissipation Concept) model but more expensive than Eddy Dissipation model.

Eddy Dissipation:

In this model overall rate of a reaction is controlled by turbulent mixing. And thus this model does not allow to incorporate any Arrhenius based finite rate. For some rapid combustion reactions this model can be used and chemical kinetics can be neglected. ANSYS FLUENT provides a model based on the work of Magnussen and Hjertager [52], called the eddy dissipation model. The rate of reaction r , $R_{i,r}$ is given by the smaller (i.e. the limiting value) of the two expressions below (Equation 3.12 and 3.13).

$$R_{i,r} = \nu'_{i,r} M_{w,i} A \rho \frac{\varepsilon}{k} \min \Re \left(\frac{Y_{\Re}}{\nu'_{\Re,r} M_{w,\Re}} \right) \quad 3.12$$

$$R_{i,r} = \nu'_{i,r} M_{w,i} A B \rho \frac{\varepsilon}{k} \left(\frac{\sum_P Y_P}{\sum_J \nu''_{j,r} M_{w,j}} \right) \quad 3.13$$

Where,

Y_P = mass fraction of any product species, P

Y_{\Re} = mass fraction of any reactant, \Re

A = an empirical constant equal to 4

B = an empirical constant equal to 0.5

k = turbulent kinetic energy

ε = turbulent dissipation rate

$\nu_{j,r}''$ = stoichiometric coefficient of the product j in reaction r

$\nu_{i,r}'$ = stoichiometric coefficient of the reactant i in reaction r

$\nu_{\mathfrak{R},r}'$ = stoichiometric coefficient of any reactant in a reaction r

$M_{w,\mathfrak{R}}$ = molecular weight any reactant, \mathfrak{R}

$M_{w,j}$ or $M_{w,i}$ = molecular weight of species i or j respectively

Chemical reaction rate is governed by the large eddy mixing time scale, $\frac{k}{\varepsilon}$. Reaction

proceeds as long as $\frac{k}{\varepsilon} > 0$. This method will allow multistep reaction but it would

calculate same rate for all the steps and results are generally inaccurate.

Eddy Dissipation Concept:

Eddy Dissipation Concept model is an extension of eddy dissipation model to include detail chemical mechanism in turbulent flows [53]. This model assumes that reactions occur in a small turbulent structure called fine scale. In ANSYS FLUENT the length fraction of the fine scale is modeled as equation 3.14

$$\xi^* = C_{\xi} \left(\frac{\nu \varepsilon}{k^2} \right)^{1/4} \quad 3.14$$

Where ,

* = denotes the fine scale quantities

C_{ξ} = volume fraction constant = 2.1377

ν = kinematic viscosity

The volume fraction of the fine scale are calculated as $(\xi^*)^3$. Species are assumed to react in the fine structure of volume $(\xi^*)^3$ over the time scale defined as the equation 3.15.

$$\tau^* = C_\tau \left(\frac{\nu}{\varepsilon} \right)^{1/2} \quad 3.15$$

where C_τ is the time scale constant equal to 0.4082. Arrhenius reactions are supposed to proceed in the fine volume $(\xi^*)^3$ over the time τ^* . Finally the rate of reaction has been modeled as equation 3.16

$$R_i = \frac{\rho(\xi^*)^2}{\tau^*[1-(\xi^*)^3]} (Y_i^* - Y_i) \quad 3.16$$

Where, Y_i^* is mass fraction of the species i after reacting in the fine structure over the time τ^* . This model can incorporate detail kinetic mechanism but typical mechanisms are invariably stiff and their solutions are computationally very expensive.

3.4.3 CHEMKIN CFD for FLUENT

CHEMKIN CFD is an add-on to the FLUENT [54]. FLUENT allows user to import finite rate kinetics in CHEMKIN format in some cases. CHEMKIN demands kinetics calculations are much faster when it is done using CHEMKIN CFD for FLUENT solver instead of “Kinetics” which is FLUENT’s stiff-chemistry solver. In usual cases there are three files needed to import into FLUENT pre-processor, i.e. reaction mechanism file, thermodynamic data and transport data to start CHEMKIN CFD solver. A reaction

mechanism file contains kinetic rate parameters such as Arrhenius factor A , temperature exponent, β and activation energy, E for each reaction. This file also allows to overwrite order of reaction from default elementary order. Parameters for pressure dependent reactions, enhance third body efficiencies can also be incorporated. Thermodynamic file contains seven temperatures co-efficient (a_{1k} to a_{7k}) in a formatted way. (Equation 3.17 to 3.19) [55]

$$\frac{C_{pk}^o}{R} = a_{1k} + a_{2k}T_k + a_{3k}T_k^2 + a_{4k}T_k^3 + a_{5k}T_k^4 \quad 3.17$$

$$\frac{H_k^o}{RT_k} = a_{1k} + \frac{a_{2k}}{2}T_k + \frac{a_{3k}}{3}T_k^2 + \frac{a_{4k}}{4}T_k^3 + \frac{a_{5k}}{5}T_k^4 + \frac{a_{6k}}{T_k} \quad 3.18$$

$$\frac{S_k^o}{R} = a_{1k} \ln T_k + a_{2k}T_k + \frac{a_{3k}}{2}T_k^2 + \frac{a_{4k}}{3}T_k^3 + \frac{a_{5k}}{4}T_k^4 + a_{7k} \quad 3.19$$

Transport properties file includes six parameters. FLUENT will calculate molecular transport property based on the following six parameters. These parameters values are needed to be included in the CHEMKIN transport properties file.

1. An index indicating whether the molecule has a monatomic, linear or nonlinear geometrical configuration. If the index is 0, the molecule is a single atom. If the index is 1 the molecule is linear, and if it is 2, the molecule is nonlinear.
2. The Lennard-Jones potential well depth, ε/k_B in Kelvins.
3. The Lennard-Jones collision diameter, σ in Angstroms.
4. The dipole moment μ in Debye. A Debye is $10^{-18} \text{cm}^3/2 \text{erg}^{1/2}$
5. The polarizability, α in cubic Angstroms.
6. The rotational relaxation collision number, Z_{rot} at 298K.

3.4.4 Models for Turbulence

The next important step is to use a proper turbulence model. ANSYS FLUENT provides several turbulence models such as

- ✓ RANS based:
 - Spalart-Allmaras model (one equation)
 - Standard k - ϵ model (two equations)
 - RNG k - ϵ model (two equations)
 - Realizable k - ϵ model (two equations)
 - Standard k - ω model (two equations)
 - SST k - ω model (two equations)
 - V2F model (four equations)
 - Reynolds Stress Model (seven equations)
- ✓ Detached Eddy Simulation
- ✓ Large Eddy Simulation

Successful turbulence modeling requires engineering judgment of flow physics, computational recourses, project requirements, accuracy required, turnaround time and choice of near wall treatment etc. Literature review shows that there is no single, superior turbulence model for all flows [52]. However in this thesis realizable k - ϵ model will be used which is computationally not very expensive and provides acceptably accurate results for combustion problem. As the name suggest this model is based on turbulent kinetic energy (k) and turbulent dissipation rate (ϵ). The term “realizable” means that model satisfies certain mathematical constrains on the Reynolds stresses with

the physics of the turbulent flows. Neither Standard k-ε or RNG k-ε models is realizable.

Transport equations for realizable k-ε model are as follows, equations 3.20 to 3.21 [52].

$$\frac{\partial}{\partial t}(\rho k) + \frac{\partial}{\partial x_j}(\rho k u_j) = \frac{\partial}{\partial x_j} \left[\left(\mu + \frac{\mu_t}{\sigma_k} \right) \frac{\partial k}{\partial x_j} \right] + G_k + G_b - p\varepsilon - Y_M + S_k \quad 3.20$$

$$\frac{\partial}{\partial t}(\rho \varepsilon) + \frac{\partial}{\partial x_j}(\rho \varepsilon u_j) = \frac{\partial}{\partial x_j} \left[\left(\mu + \frac{\mu_t}{\sigma_\varepsilon} \right) \frac{\partial \varepsilon}{\partial x_j} \right] + \rho C_1 S \varepsilon - \rho C_2 \frac{\varepsilon^2}{k + \sqrt{\nu \varepsilon}} + C_{1\varepsilon} \frac{\varepsilon}{k} C_{3\varepsilon} G_b + S_\varepsilon \quad 3.21$$

Where, $C_1 = \max \left[0.43, \frac{\eta}{\eta + 5} \right]$ and $\eta = \frac{Sk}{\varepsilon}$ where $S = \sqrt{2S_{ij}S_{ij}}$

G_k = generation of turbulent kinetic energy due to mean velocity gradients

G_b = generation of turbulent kinetic energy due to buoyancy

Y_M = contribution of the fluctuating dilatation in compressible turbulence to overall

dissipation rate. C_2 and $C_{1\varepsilon}$ are constants. σ_k and σ_ε are the turbulent Prandtl number for

k and ε respectively. S_k and S_ε are user defined source terms.

3.5 ANSYS FLUENT Solver Basics

ANSYS fluent has two different flow solvers, namely pressure based solver and density based solver. These two solvers differ in the way that the continuity, momentum energy and species equations are solved. Two pressure based solver algorithms are available in ANSYS FLUENT. They are pressure based segregated solver and pressure based coupled solver. Algorithms for different solvers have been attached to Appendix A.

Figure A.1 and A.2 show the algorithms for these two types of pressure based solvers. In density based solver two types of formulation are available: implicit and explicit formulation for coupled system of equations (continuity, momentum, energy, species etc.). Figure A.3 shows the algorithm for density based solver. Pressure based solver traditionally has been used for incompressible and mildly compressible flows [50] whereas density based solver was originally designed for high-speed compressible flows. However they have been modified such that, nowadays, both of the solvers can be used independent of flow physics [52].

3.6 Solution Methods

Under solution method ANSYS FLUENT provides different types of discretization in terms of spatial and also temporal for unsteady flow calculation. Major spatial discretization schemes include but not limited to

- First-order Upwind Scheme
- Power-Law Scheme
- Second order Upwind Scheme
- First to higher order blending
- Third-order MUSCL scheme

3.7 Solution Controls

Solution Control is mainly done changing Under-Relaxation factor and Courant Number in pressure based and density based solver respectively. Initially small under-relaxation and courant number are used to stabilize the solver. But in the later run these values are increased slowly to get better convergence.

3.8 Solution Initialization

Solution must be initialized before one starts iterations. Initialization process puts some values in every cell in order to start iteration from. ANSYS FLUENT provides different boundary zone based initializations which are useful in small CFD simulations. But these initialization processes may take long time to converge the solution as boundary values are far from the actual solution in the domain.

3.9 Convergence Check and Residuals

Checking that, whether the solution has converged or not is very crucial in CFD simulation. Several ways to check the convergence may include but are not limited to

1. Checking whether continuity equation satisfies over the whole fluid volume
2. Checking whether energy equation satisfies over the whole fluid volume
3. Checking the level of residuals
4. Whether residuals are constant at the final iterations stage.
5. Compare the results with experimental values

Procedures for checking continuity can be checking the net mass flow rate through boundaries. If the net mass flow rate is zero or close to zero, then the requirement of continuity equation has been met and solution may have converged. The same formula must apply to check energy conservation. If the net heat flow rate through all the boundaries is zero or close to zero then the solution may have converged.

Another procedure to check convergence is checking the level of residual. For pressure based solver ANSYS FLUENT defines the residual by the following equation 3.22 [50].

$$R^\phi = \sum_{cells} (|e^\phi|) \quad 3.22$$

Where, e^ϕ is the imbalance or error involved associated with a balance equation computed in a particular cell. When the absolute value of this imbalance is summed over the whole computational domain the obtained value, R^ϕ is called residual for a particular balance equation, ϕ . For particular conservation variable ϕ , the discrete equation at any cell P can be written as equation 3.23,

$$a_p \phi_p = \sum_{nb} a_{nb} \phi_{nb} + b \quad 3.23$$

Where a_p is center coefficient for a particular variable ϕ_p for a particular cell, P .

a_{nb} is the influence coefficient for a neighboring cell,

ϕ_{nb} is conservation variable corresponding to that neighboring cell

nb is the number of neighboring cells involved with cell P

b is influence of sources terms on ϕ_p .

Rearranging the equation 3.23 the expression for imbalance e^ϕ in cell can be computed as equation 3.24.

$$e^\phi = \sum_{nb} a_{nb} \phi_{nb} + b - a_p \phi_p \quad 3.24$$

Finally residual is obtained as sum of absolute values of such imbalances, e^ϕ over the whole computational domain. (Equation 3.25).

$$R^\phi = \sum_{cells} \left(\left| \sum_{nb} a_{nb} \phi_{nb} + b - a_p \phi_p \right| \right) \quad 3.25$$

CHAPTER 4

PROBLEM SET-UP AND SOLUTION

4.1 Introduction

The primary objective of this chapter is to formulate the problem step by step, set it up, and solve it. Our objective is to predict, mainly, NO_x formation in an aircraft engine using CFD simulation. NO_x is a combustion product which forms at high temperature during oxidation of jet fuel. Modeling of such system must require a chemical kinetic scheme for oxidation of jet fuel which is to be properly selected. Although model verification should come afterward, reconsiderations have been given due to limited availability of information for such case. APEX (Aircraft Particle Emission eXperiment) campaign data has been chosen for model verification [7]. And thus, depending on the availability, operating conditions were taken consistently for a harmonious comparison. However different simplifying assumptions must be made to develop a computationally viable model (i. e. a model can be solved using current computation facility). Other than the computational limitations, assumptions were necessary for information protected by commercial patent protection. The original APEX campaign emission data are available on a McDonnell Douglas DC-8 which is a military aircraft run by CFM-56-2C1 engine. The information such as fuel injection system, overall residence time of combustion products in the chamber, primary zone air-fuel ratio, number of holes and flow rate per hole etc. are protected by the manufacture patent and this information is not open to

public. However, these variables must affect the NO_x formation prediction and are need to be assumed properly.

In this thesis first of all a combustion chamber is developed to mimic an aircraft engine combustion process. Although the post-combustion process may affect emission prediction [5], here, we will assume that there are no further changes in species concentrations after the gas mixture leaves combustor exit. After designing the combustion chamber, it has been meshed and solved computationally with boundary conditions extracted from Wey et al [7]. In the subsequent sections these steps will be discussed.

4.2 Modeling of Combustion Chamber

Design of the combustion chamber is critical for accurate modeling of emission prediction. Modern aircraft engine combustion chamber (figure 2.2, 2.5(a)) can be either conical or annular. However the basics of flow process inside chamber is that some primary air with fuel are injected into the combustion chamber. This primary air may also be called swirling air and used to vaporize and inject the fuel into the main combustion chamber. Detail design of injection system is highly complicated and here we will use an annular injection system. However in actual engine liquid fuel and swirling air creates a premixed air/fuel mixture and which is injected into the chamber. Here we will avoid discrete phase modeling associated with injection of liquid fuel. Because in that case computer has to handle lots of discrete particles and model gets even bulkier. Under this circumstance discrete phase modeling usually comes as a separate study from original

combustion simulation, although NO_x formation is not independent of injection technology [13]. After this initial air/fuel injection into the primary burning zone of the combustion chamber, secondary air, to complete the combustion and dilution air, to cool the mixture down before it goes to turbine are also added through a series holes throughout the length of the combustion chamber. However these flow rates and sizing of the chamber are proprietary information of engine manufacturer and they are not open to public. Here we shall design a cylindrical combustion chamber with annular injection system. Flow rate will be adjusted such that the residence time for gas mixture inside the chamber is around 10ms. Figure 4.1 shows computer representation (XZ plane view) of the designed chamber. ‘ANSYS Design Modular’ has been used to draw the chamber. Axis of this chamber is Z-axis and extends from Z=1.5 cm to 25 cm. For better illustration purpose, the following zones can be named based on Z coordinate.

$Z = [1.5:4.0]$ cm → Burner-up

$Z = [4.0:4.5]$ cm → Injection

$Z = [4.5:25.0]$ cm → Flame Holder

Burner-up is a cylindrical fluid volume with 6cm inlet and outlet diameter. The length of this zone is 2.5cm. Injection system starts right after burner-up. The injection system extends from 4.0cm to 4.5cm. Figure 4.2 shows view of the plane cut perpendicular to the Z-axis at Z=4.25cm. Practically this view would be same for plane cut perpendicular to the Z-axis for any $Z = [4.0:4.5]$ cm. Three annular injection system has created with 0.55cm annular thickness.

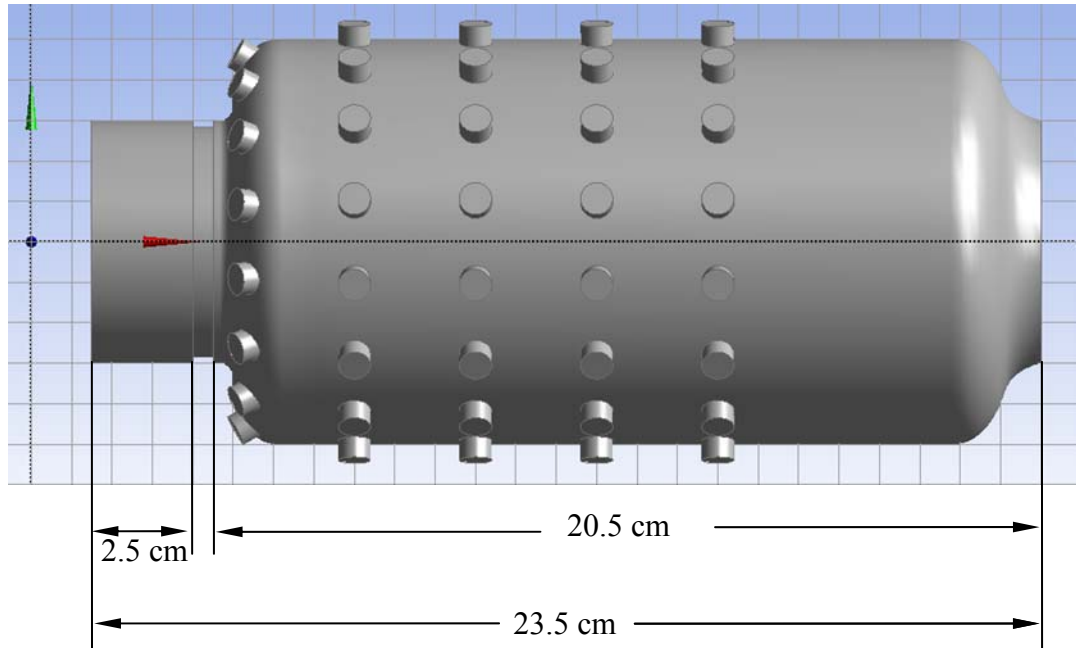


Figure 4.1 Computer representation of combustion chamber geometry.

In figure 4.2

$R_7 = 0.3\text{cm}$, $R_8 = 0.85$ and $(R_8 - R_7) = 0.55\text{cm}$ (for inner injection)

$R_9 = 1.3\text{cm}$, $R_{10} = 1.85$ and $(R_{10} - R_9) = 0.55\text{cm}$ (for middle injection)

$R_{11} = 2.3\text{cm}$, $R_{12} = 2.85$ and $(R_{12} - R_{11}) = 0.55\text{cm}$ (for outer injection)

Whereas the radius of the outer-most circle is 3 cm.

Finally, flame holder is a cylindrical chamber with slightly converging and diverging at the ends. Both inlet and outlet diameters are 6cm. Maximum diameter of the chamber is 10cm. The flame holder extends 17cm with maximum diameter. The flame holder has 80 holes periodically arranged across its length and radial directions. Each of them has uniform diameter of 0.8cm. Along the axis it has five sets of holes. Each set contains 16 holes periodically arranged along the circumferences of the flame holder. Angular distance between two consecutive holes is 22.5° . Axial positions of the holes are $Z = 5.5, 8,$

11, 14, 17cm. The first set of holes at $Z=5.5\text{cm}$ makes 30° angle with Z-axis (axis of the chamber). However other four sets are perpendicular to Z axis. In figure 4.1 the holes are shown as extended material for better visualization purpose. However in the actual modelling they will appear as imprint (i.e. separate) surfaces (figure 4.3).

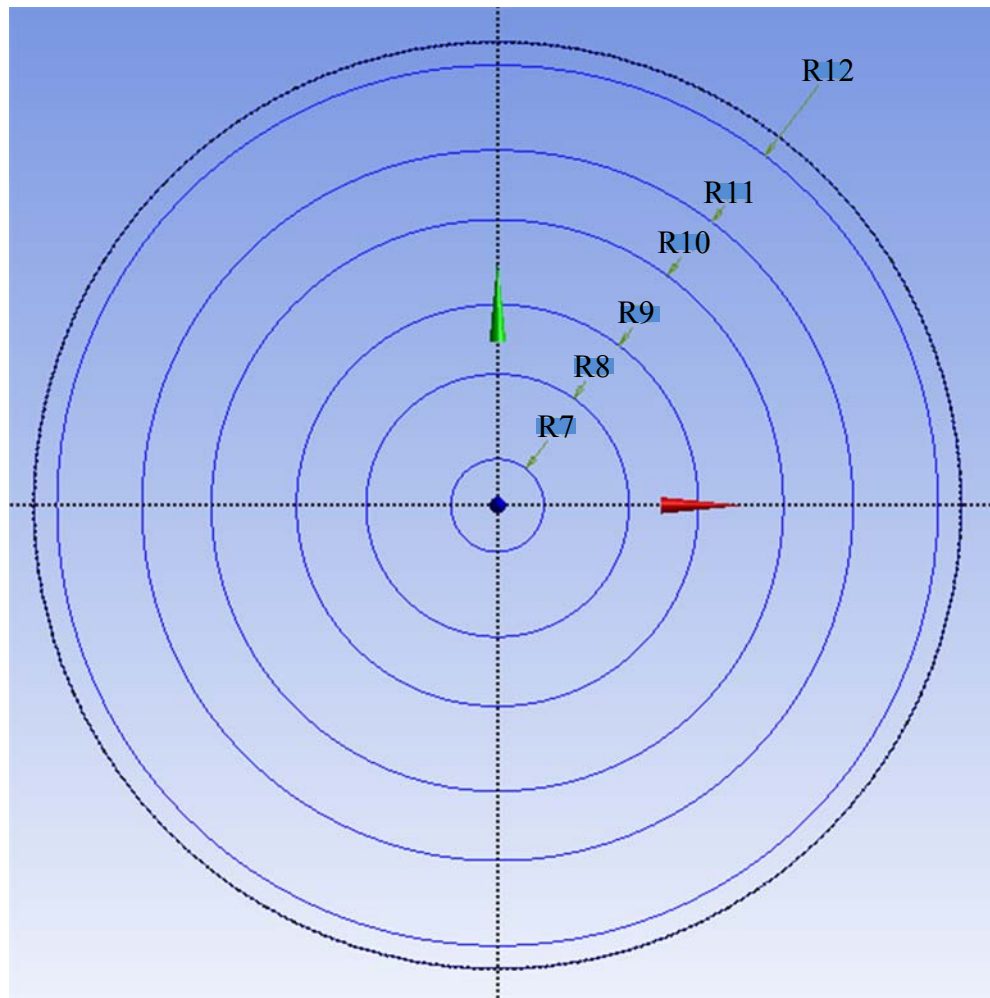


Figure 4.2 Cross-section of injection system.

As our designed chamber is rotatinally periodic with an angle of period 22.5° , it is not necessary to simulate the complete chamber, instead, we can simulte only $1/16^{\text{th}}$ part of the complete chamber. That will significantly reduce the computational time (i.e. at least 16 times faster). After cutting the geometry, figure 4.3, two new planes found has been set as rotationally periodic. However in the figure 4.3 several boundary zones are shown with names as used in the fluent setup.

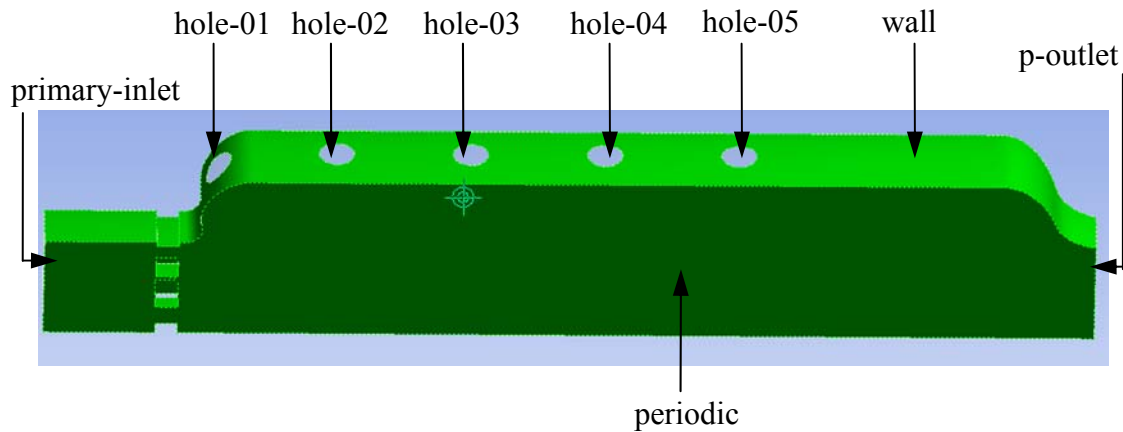


Figure 4.3 Fluid volume considered for simulation.

4.3 Meshing

Meshing is a very important part in CFD simulation. Without a proper mesh, it will not be possible to get converged solution. In this thesis meshing has done using ANSYS Meshing feature. Major mesh setting variables include the following-

Physical reference	CFD
Solver Preference	FLUENT
Relevance	-100

Use Advanced Size Function	On: Curvature
Relevance Center	Coarse
Shape Checking	CFD
Smoothing	Medium
Transition	Slow
Span Angle Center	Fine
Minimum Size	Default
Maximum Size	Default
Defeaturing Tolerance	1E-07

After these initial settings, ‘Match control’ operation must be applied to the two periodic planes in order to replicate the meshing nodes in both surfaces. In addition to that boundaries are renamed as shown in figure 4.3. Naming of boundaries includes, primary-inlet, hole-01, hole-02, hole-03, hole-04, hole-05, periodic, periodic-s, p-outlet, wall. In actual simulation these boundaries were defined as follows-

primary-inlet	mass flow inlet
hole-01	mass flow inlet
hole-02	mass flow inlet
hole-03	mass flow inlet
hole-04	mass flow inlet
hole-05	mass flow inlet
p-outlet	outflow
wall	wall

‘periodic’, and ‘periodic-s’ are set as rotationally periodic boundary using text user interface. Then one of the boundaries will be deleted and merged with other one to make the faces as periodic boundary. Finally the mesh generation command can be executed to get the gridded geometry (Figure 4.4) which shows high density of cell near curvature and small surfaces (injection, holes). This is because, advanced size function was turned on and Masher automatically detects complexity of the geometry and puts more cells near those areas.

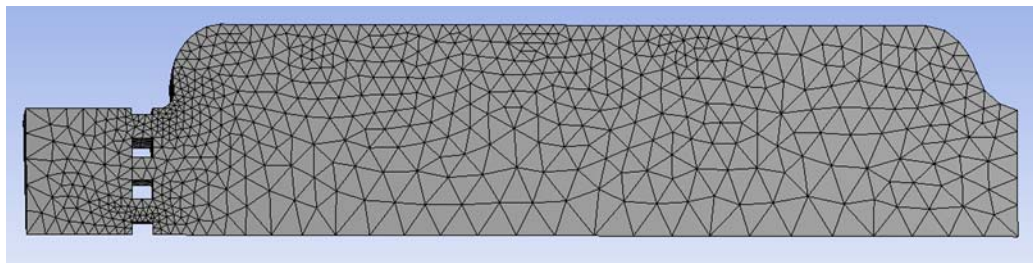


Figure 4.4 Meshed geometry.

After mesh generation, the cells were checked to observe the orthogonal quality and skewness. If those values are not inside the recommended values, the mesh was remeshed. For these mesh settings it produced 14,799 tetrahedron cells with 3450 nodes. Figure 4.5 shows skewness metrics of the generated mesh. According to the table 3.1 the mesh is acceptable. It also shows maximum skewness is 0.87. Whereas figure 4.6 shows the orthogonal quality spectrum and it shows minimum orthogonal quality for this mesh is 0.36 which is also between acceptability limits according to table 3.1. Also grid

independence study has been done with a global kinetic scheme and the mesh has been verified.

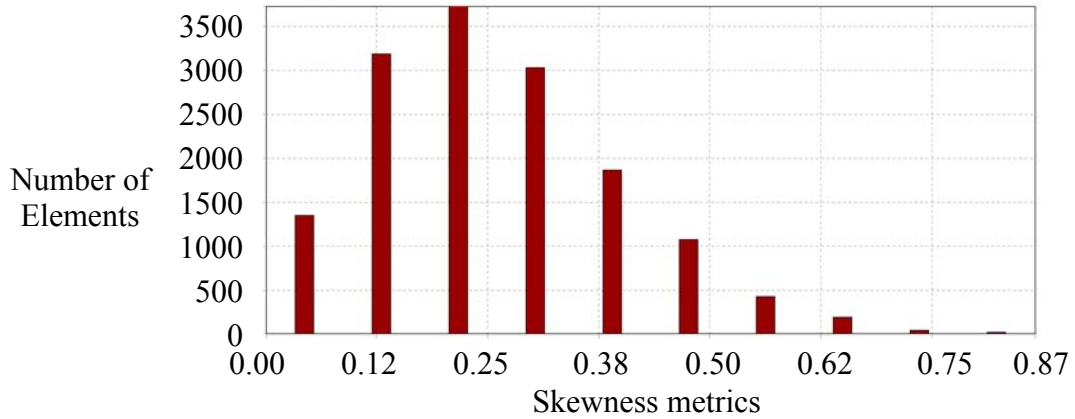


Figure 4.5 Skewness metrics for the generated mesh.

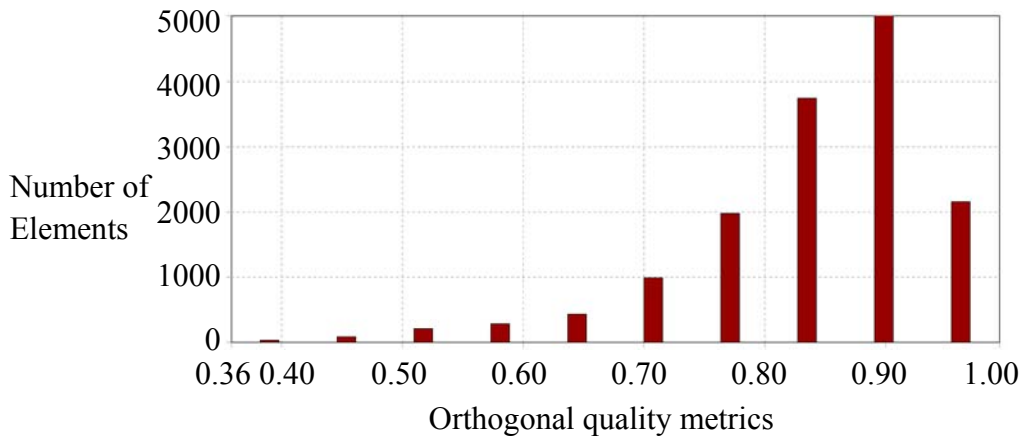


Figure 4.6 Orthogonal quality metrics for the generated mesh.

4.4 Test Matrices

Before, we actually set-up the boundary conditions in FLUENT, it is imperative to discuss the problem formulations. As our objective, initially described, was to compare with the APEX measured emission data, problem will be formulated taking some known parameters such as engine air fuel ratio, fuel flow rate, combustor inlet temperatures and pressures, humidity of atmospheric air etc. from Wey et al at [7]. After that emission level will be compared with their measured data for corresponding engine settings.

APEX campaign emission data are available for different test point with different engine power setting [7]. These emission data were also obtained at different weather conditions. Exhaust gas was collected and analyzed for emission measurement. Figure 4.7 shows the schematic of multiport sample rake used at APEX campaign emission measurements [7].

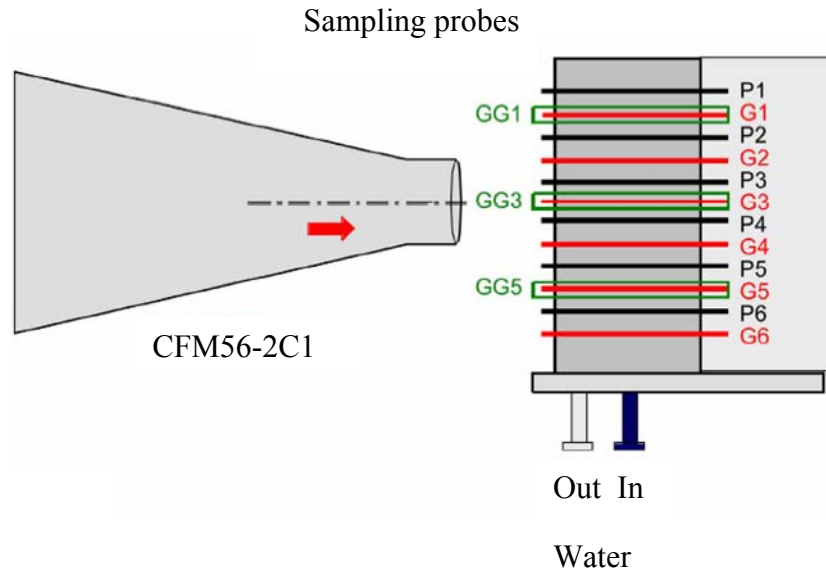


Figure 4.7 Sample rake with 6 (G1-G6) gas, 6 (P1 to P6) particle and six external (GG1 to GG6) sample probes.

Sampling probes were placed 1m, 10m, and 30m from to the exhaust plume. However, in this thesis, we will assume that no further reactions occur between gas mixtures after it exits from the combustion chamber so that we fairly can take emission data of the probe 1m down from the exhaust plume for comparison. To observe spatial variation along radial direction multi-port particle and gas sample rakes were also used.

For our simulation we shall pick up four different engine power setting that will mimic LTO cycle defined by ICAO near airport [9]. However test points are considered randomly from the available engine power settings. Table 4.1 shows test point number with probe number for which APEX campaign emission data are considered for comparisons.

Table 4.1 Test matrices under consideration.

Test Point	Probe Number	Engine Power
613	R1G3	7% (idle/taxi)
521	R1G3	30% (approach)
506	R1G3	85% (climb)
523	R1G2	100% (take-off)

In table 4.1, R1 means the probe at 1m down from the exhaust plume and G3 is gas probe at the center of that plume (Figure 4.7). However spatial variation of emission along radial direction is very small and any of these values can be taken as average values [7].

4.4.1 Combustor Inlet Temperature and Pressure

In order to solve our CFD model we need adequate boundary conditions such as, mass flow rate, operating pressure, inlet temperature and fuel air ratio etc. Table 4.2 shows some operating conditions obtained from Wey et al [7] for the CFM-56-2C1 engine.

Table 4.2 Operating conditions for CFM-56-2C1 engine.

Test Point Probe-No Engine Power	Cumulative Fuel Air Ratio at Combustor Exit (by mass)	Engine Fuel Flow Rate, kg/s	P3norm	T3norm
613- R1G3-7%	0.0128	0.115	0.15	0.628
521-R1G3-30%	0.0124	0.275	0.358	0.81
506-R1G3-85%	0.0172	0.724	0.777	0.99
523-R1G2-100%	0.0201	0.850	0.816	1.019

P3norm and T3norm are normalized combustor inlet pressure and temperature with respect to a value for the same variable that would be observed when the engine would run at 100% rated power on standard day condition. For pressure such value is engine pressure ratio. Engine pressure ratio for CFM56-2C1 engine, maximum pressure (atm) at the compressor outlet (i.e. when engine runs at 100% rated thrust), is 23.5. The corresponding temperature can be taken as maximum temperature at the compressor outlet. For example P3norm for the test point 523 in the above table is 0.816, so the actual combustor inlet pressure would be 23.5 times 0.816 equal to 19.17 atm. Operating pressure for rest of engine power setting can be calculated is the same way. However no

such maximum values for temperature can be found in the engine manufacturer data sheet or in Wey et al [7]. But this value is calculated using following thermodynamic relation for gas compression pressure temperature relation (Equation 4.1) [56].

$$T_2 = T_1 \left[1 + \frac{\left(\frac{p_2}{p_1} \right)^{\frac{\gamma-1}{\gamma}} - 1}{\eta} \right]. \quad 4.1$$

Where T_1 is the ambient temperature of a standard day, 288.15K [7] and compressor efficiency η can be taken as 0.9. $\frac{p_2}{p_1}$ is the engine pressure ratio, 23.5. γ is taken as

1.41. Thus maximum temperature T_2 can be calculated using this above equation 4.1

Once T_2 (= 784.4K, when multiplied with T3norm for 100% power setting) is found, after multiplying with T3norm combustor inlet temperature has also been found. Finally combustor inlet temperature and pressure are summarized in the Table 4.3.

Table 4.3 Combustor inlet temperature and pressure.

Test Point Probe-No Engine Power	Combustor inlet temperature (K)	Combustor inlet pressure (Pa)
613- R1G3-7%	492.60	357171
521-R1G3-30%	635.36	852447
506-R1G3-85%	776.55	1850144
523-R1G2-100%	784.39	1943008

4.4.2 Calculation of Combustor Air Flow Rate

Combustion air flow rate can be calculated with the help of fuel air ratio and engine fuel flow rate. Table 4.4 summarizes air flow rate for different operating condition.

Table 4.4 Combustor air flow rate.

Test Point Probe-No Engine Power	Cumulative Fuel Air Ratio at Combustor Exit (by mass)	Engine Fuel Flow Rate, kg/s	Air Flow Rate, kg/s
613- R1G3-7%	0.0128	0.115	8.98
521-R1G3-30%	0.0124	0.275	22.18
506-R1G3-85%	0.0172	0.724	42.09
523-R1G2-100%	0.0201	0.850	42.29

4.5 Obtaining Boundary Conditions

In relation to our simulations mass flow rates of table 4.4 are adjusted to make that appropriate for boundary conditions. Here we assume that real engine combustion chamber flow capacity is 48 times of our designed geometry. However as we are simulating 1/16th of a chamber using rotationally periodic boundary condition, total flow rate in the simulation would be 48×16 times smaller than the actual engine. As discussed earlier a premix air/fuel mixture will be injected into the primary zone (primary-inlet in figure 4.3). Primary zone equivalence ratio is obtained from figure 2.5 (b). Assumption has been made that CFM56-2C1 engine has operating conditions similar to V2500

Burner. Table 4.5 shows primary zone equivalence ratios used for different engine power settings.

Table 4.5 Primary zone equivalent ratios for different power settings.

Engine Power Settings	Equivalence ratio in 'primary-inlet'
7%	1.10
30%	1.10
85%	1.40
100%	1.70

In table 4.5 equivalence ratio is defined as the ratio of two ratios: 'fuel to air mass ratio' to 'fuel to air stoichiometric mass ratio.' As we shall use $C_{12}H_{23}$ as the surrogate fuel, it can be shown that 'fuel to air stoichiometric mass ratio' is 0.0677. With help of table 4.5 'fuel to air mass ratio' in the 'primary-inlet' can easily be calculated. As all the fuel (i.e. fuel flow rate in table 4.4 when divided by 48×16) is injected through 'primary-inlet', associated air flow rate in the 'primary-inlet' can also be easily calculated. Once primary air flow rate is found secondary and dilution air flow can be obtained by a simple subtraction of 'primary-inlet' air flow from the total air flow (i.e. air flow rate in table 4.4 when divided by 48×16). Secondary and dilution air flow through the five holes along the length of the simulated part of designed combustion chamber. Air flow distribution through these holes is given in table 4.6. This distribution has been found by trial and error. At this distribution fuel and air reacts consistently for all engine operating

condition. For example if the ‘ hole-01 ’ gets more flow than 4%, it does not stabilize the flame in the flame-holder for 7% and 30% engine power settings. However our objective was to keep flow rate a constant percent through the different holes for different engine operating conditions. Reasoning for such approach was to keep the model consistent for different engine power setting.

Table 4.6 Secondary and dilution air flow distribution.

hole-01	hole-02	hole-03	hole-04	hole-05
04%	10%	21%	31%	34%

Table 4.7 shows some additional data obtained from Wey et al [7] related to weather conditions and engine exhaust conditions. Humidity data is used to obtain accurate air composition. It was assumed that dry air is 0.23/0.77 mixture of O₂/N₂ by mass.

Table 4.7 Ambient conditions with engine exhaust plume temperature.

Ambient Pressure, Pa	Ambient temperature, K	Molar Humidity of Air	Exhaust plume Temperature, K
94085	296	0.0043	737
93654	305	0.0030	789
93815	301	0.0043	994
93587	305	0.0030	1060

Finally, mass flow rates for different boundaries has been summarized in table 4.8 to 4.11. Also given are operating pressures and temperatures of all inlet flow streams.

Table 4.8 Flow variables for 7% engine power setting, operating pressure 357171 Pa and inlet temperature 492.6 K.

Boundary	Flow Rate, kg/s	O ₂ mass fraction	H ₂ O (v) mass fraction	C ₁₂ H ₂₃ mass fraction
primary-inlet	0.00217	0.2135	0.0025	0.0691
hole-01	0.00039	0.2294	0.0027	--
hole-02	0.00097	0.2294	0.0027	--
hole-03	0.00203	0.2294	0.0027	--
hole-04	0.00300	0.2294	0.0027	--
hole-05	0.00329	0.2294	0.0027	--

Table 4.9 Flow variables for 30% engine power setting, operating pressure 852447 Pa and inlet temperature 635.36 K.

Boundary	Flow Rate, kg/s	O ₂ mass fraction	H ₂ O (v) mass fraction	C ₁₂ H ₂₃ mass fraction
primary-inlet	0.00518	0.2137	0.0017	0.0691
hole-01	0.00096	0.2296	0.0019	--
hole-02	0.00241	0.2296	0.0019	--
hole-03	0.00505	0.2296	0.0019	--
hole-04	0.00746	0.2296	0.0019	--
hole-05	0.00818	0.2296	0.0019	--

Table 4.10 Flow variables for 85% engine power setting, operating pressure 1850144 Pa and inlet temperature 776.55 K.

Boundary	Flow Rate, kg/s	O ₂ mass fraction	H ₂ O (v) mass fraction	C ₁₂ H ₂₃ mass fraction
primary-inlet	0.01092	0.2096	0.0024	0.0863
hole-01	0.00179	0.2294	0.0027	--
hole-02	0.00449	0.2294	0.0027	--
hole-03	0.00942	0.2294	0.0027	--
hole-04	0.01391	0.2294	0.0027	--
hole-05	0.01525	0.2294	0.0027	--

Table 4.11 Flow variables for 100% engine power setting, operating pressure 1943008 Pa and inlet temperature 784.39K.

Boundary	Flow Rate, kg/s	O ₂ mass fraction	H ₂ O (v) mass fraction	C ₁₂ H ₂₃ mass fraction
primary-inlet	0.01075	0.2059	0.0017	0.1030
hole-01	0.00182	0.2296	0.0027	--
hole-02	0.00454	0.2296	0.0027	--
hole-03	0.00954	0.2296	0.0027	--
hole-04	0.01409	0.2296	0.0027	--
hole-05	0.01545	0.2296	0.0027	--

4.6 Problem Set-Up

The mesh created described earlier was loaded into FLUENT run by a DELL T3500 quad machine with 2.26GHz processor speed. Double precision solver was used. All the 4 processor were utilized to get the advantage of parallel computing speed. The mesh has been checked first. After mesh check was done by FLUENT, the following steps were followed to complete the setup.

1. Steady state, pressure based solver, absolute velocity formulation was selected.
2. Energy Equation was turned on.
3. 'k- ϵ ' (realizable) turbulence model is selected with advanced wall function.
4. Species transport model with volumetric reaction was selected
5. Eddy-Dissipation concept model was selected for turbulence kinetics interaction.
6. CHEMKIN [55] file was imported together with thermodynamic and transport files a for jet-A ($C_{12}H_{23}$) kinetics based on Kundu et al [14]. Formatted kinetics, thermodynamic and transport files have been attached in Appendix B.
7. 'primary-inlet', 'hole-01', 'hole-02', 'hole-03', 'hole-04' and 'hole-05' all the inlet were set as mass flow inlet. 'periodic' and 'periodic-s' are set as rotationally periodic boundaries through FLUENT text interface. 'p-outlet' was set as 'outflow' boundary.
8. Initial values for turbulent intensity were assumed 10% and hydraulic diameter for 'primary-inlet' is 0.06m and for all the holes 0.008m.
9. Mass fraction and flow rates are set accordingly i.e. depending on the engine power settings.

10. Operating pressure is set.

11. The following discretization scheme are selected for the corresponding variables

Pressure velocity Coupling	Simple
Gradient	Least Square cell Based
Pressure	Standard discretization scheme
Momentum	First-Order-Upwind
Turbulent Kinetic Energy	First-Order-Upwind
Turbulent Dissipation Rate	First-Order-Upwind
Turbulent viscosity	First-Order-Upwind
Species	First-Order-Upwind
Energy	First-Order-Upwind

12. The following under-relaxation values were used for initial iterations

Pressure	0.3
Density	1
Body Forces	1
Momentum	0.7
Turbulent Kinetic Energy	0.8
Turbulent Dissipation Rate	0.8
Turbulent viscosity	1
Species	0.5
Energy	0.5

13. The solution is initialized from 'primary-inlet' boundary.

14. After 400 'cold flow iteration' solution domain was ignited at 1500K for all $Z=[0.05:0.10]$ m.
15. After Additional 1200 iteration, under-relaxation values for energy and species were increased at 0.9.
16. Additional 800 iterations were run to get the final solution.

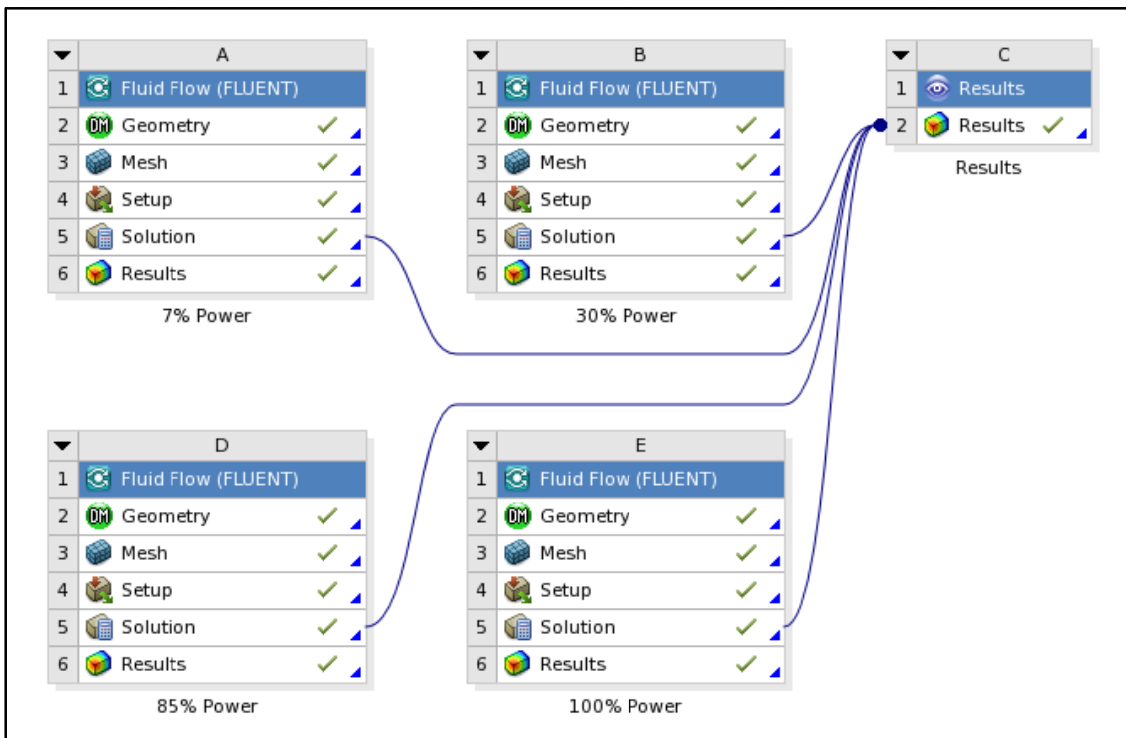


Figure 4.8 Workflow in FLUENT Workbench.

After completing all the steps the results are ready to post-process. These steps has been repeated for all four engine power settings. The post-processing was done by transferring the all the solution files in a single 'Result' block of FLUENT. Figure 4.8 shows the workflow in the FLUENT Workbench.

4.7 Convergence Check

Solution convergence check is a very important step in CFD simulation. It has been suggested that, when residuals get constant for at least 50 iterations the solution may have converged [51]. However many more than 50 (approximately 300) were run at constant residuals to confirm the stable solutions. At the same time, levels of residuals were checked to verify convergence. However, as it is a steady state simulation, at converged position the solver will give constant values for any variables at fixed position inside computational domain. In this case, average facet values for static temperature are also observed at the outlet throughout the calculation. In Appendix C two sets of figures has been attached. The first set of figures (C.1 to C.4), show convergence monitor of static temperature at outlet. From these figures, it is discernible that, steady values are obtained for all the cases. Second sets (figures C.5 to C.8) plot residuals. From these figures level of residuals can be observed for different conserved equations throughout the whole calculation. For energy equations residuals are well below ANSYS Inc., recommended value, $1e-6$ [51]. For species and other equations, residuals are below $1e-3$ which also suggests well converged solution. Another basic factor must be checked is whether net mass flow and heat flow rates through different boundaries are zero or at least close to

zero. Table 4.12 shows such values at converged positions and the values agree proving proper convergence.

Table 4.12 Net Mass and Heat flow rate at converged position.

Test Point	Net mass flow rate, kg/s	Net heat flow rate ,W
613-7% Power	-4.33E-19	1.62
521 -30% Power	1.30E-17	3.86
506 -85% Power	6.93E-18	5.71
523 -100% Power	3.47E-18	0.87

CHAPTER 5

RESULTS AND DISCUSSION

5.1 Introduction

It took nearly 5hr CPU time to get the converged solutions for each of these engine settings. It has also been observed that CPU time increases proportionally with number of cells in the computational domain. However increases in number of species affects the computational time nonlinearly. Computational time variation due to number of species variation, approximately, can be expressed as proportional to n^b , where n is number of species and b is between 2 and 3. Other factors such as under-relaxation factor, discrete scheme used etc. can also affect the time of computation.

In this chapter we shall compare the emission predicted from this model and emission measured by APEX campaign. Different contour plot of different variables will be visualized to understand the physics and chemistry of the model.

5.2 Comparison of NO_x Emission

In our model NO_x is comprised of NO and NO₂ according to the kinetic scheme used in this simulation [14]. Our results for NO_x are compared with APEX campaign emission results (Table:5.1). Although there is large discrepancy for test point 521, the rest of the data agrees fairly well with experimentally measured data. However in this model, the NO_x emission rate does not follow any trend, on the other hand, in APEX measured data, NO_x emission usually increases with engine power settings.

Table 5.1 NO_x emission comparison for this model with APEX measured data.

Case & Test-point, power and probe number	APEX measured, NO _x , g/kg fuel	This model NO _x =(NO+N ₂ O), g/kg fuel
613 -7%- R1G3	3.86	7.12
521 -30%- R1G3	9.29	19.31
506 -85%- R1G3	16.39	16.95
523-100%- R1G2	18.39	13.38

5.3 Comparison of N₂O Emission

The amount of N₂O emission is negligible compared to total amount of NO_x. But N₂O is an important intermediate in NO_x chemistry. This model predicts N₂O formation for the test point 613 and 521 as good agreement with APEX data (table 5.2). For the other two test points predicted N₂O emission is somewhat higher than for APEX test points.

Table 5.2 N₂O emission comparison for this model with APEX measured data.

Case & Test-point, power and probe number	APEX measured, N ₂ O, g/kg fuel	This model N ₂ O, g/kg fuel
613 -7%- R1G3	0.088	0.131
521 -30%- R1G3	0.101	0.158
506 -85%- R1G3	0.064	0.303
523-100%- R1G2	0.062	0.339

5.4 Comparison of CO Emission

The model is highly inconsistent for CO emission prediction (Table 5.3). It shows reduction of CO from test-point 613 and 521. Then it increases for test-point 506 and 523. The APEX data on the contrary shows a steady reductions of CO from 7% engine power to 100% engine power.

Table 5.3 CO emission comparison for this model with APEX measured data.

Case & Test-point, power and probe number	APEX measured, CO, g/kg fuel	This model CO, g/kg fuel
613 -7%- R1G3	34.46	76.13
521 -30%- R1G3	5.14	33.23
506 -85%- R1G3	1.39	64.17
523-100%- R1G2	1.89	147.09

5.5 Comparison of CH and C₂H₂ Emission

Whereas the model gave high predictions for CO emissions, CH and C₂H₂ emissions were found to be negligible compared to APEX data. Results for CH and C₂H₂ emissions are shown in table 5.4 and 5.5.

Table 5.4 CH emission comparison for this model with APEX measured data.

Case & Test-point, power and probe number	APEX measured, CH, g/kg fuel	This model CH, g/kg fuel
613 -7%- R1G3	0.96	0.010351
521 -30%- R1G3	0.6	0.000693
506 -85%- R1G3	0.64	0.000001
523-100%- R1G2	0.76	0.000000

Table 5.5 C₂H₂ emission comparison for this model with APEX measured data.

Case & Test-point, power and probe number	APEX measured, C ₂ H ₂ , g/kg fuel	This model C ₂ H ₂ , g/kg fuel
613 -7%- R1G3	0.109	4.909E-11
521 -30%- R1G3	0.025	3.994E-13
506 -85%- R1G3	0.021	2.419E-13
523-100%- R1G2	0.027	1.956E-10

5.6 Contours of Different Variables

In this section different contour are plotted for all four engine power settings. Global scale (i.e. same scale for all four cases) has been used for a single variable. These contours are drawn in plane that makes 11.25° angle with Z-axis, where in our original geometry (figure 4.3) similar planes (i.e. two periodic planes) create 22.5° with each other. In that sense this plane would be a divider of the periodic planes. 3D scenario of variable can approximately be taken by rotating this plane about z-axis by 360° . In this section, temperature, velocity, CO mass fraction, NO mass fraction and flow direction's counters are presented. Comments have been made on variations of these variables for different power settings.

Temperature variations have been plotted for different engine power settings and these plots show that, as fuel to air ratio and inlet temperature increase with increase in engine power, faster burning and higher average temperature for higher engine power settings. From CO mass fraction contours, high CO concentration zones are visible for higher engine power settings. NO mass fraction contours show that there is no uneven NO distribution or high NO production in certain region of the chamber. Plots of other variables such as density, total pressure and other major, minor species are attached in Appendix D.

5.6.1 Temperature Contours

Figures 5.1A to 5.1D, show temperature profiles for different engine power settings. High temperature is observed at the neck and center of the burner. However this intensity increases with the increases in engine power. In addition to that high temperature burning zones move close to the injection plane as the engine power increases. The main reason for this faster burning as the engine power increases is due to increase in combustor inlet temperature. Overall the four figures (5.1A to 5.1D) show similar burning profile for all the power conditions.

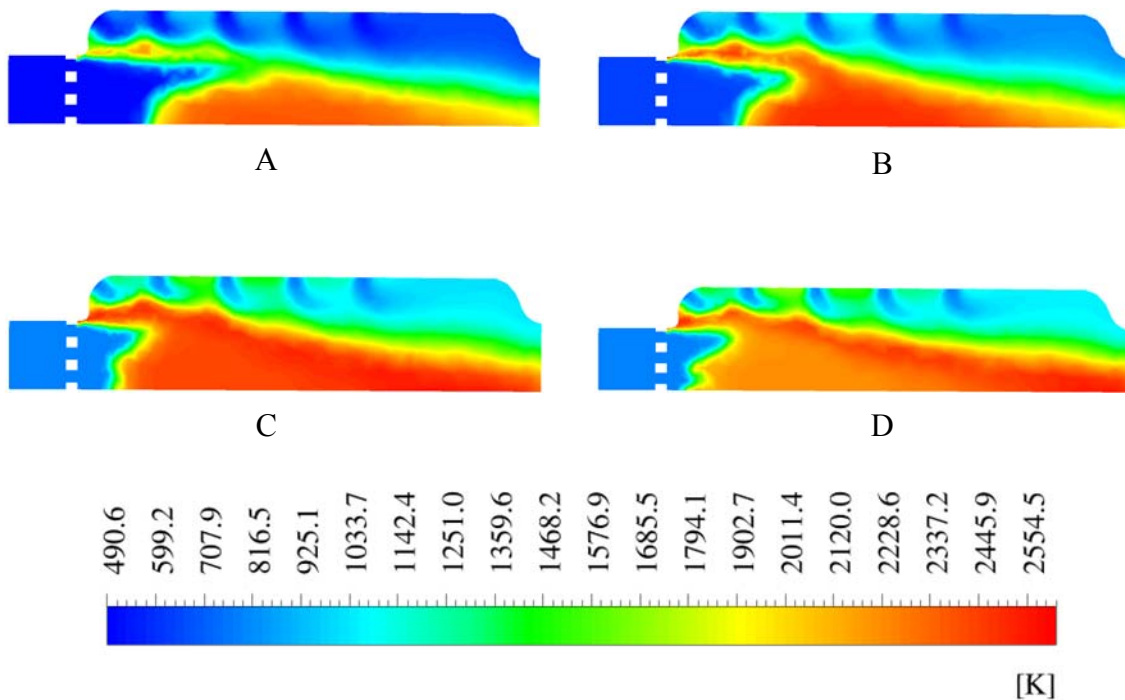


Figure 5.1 Temperature profile. A: 7% power, B: 30% power, C: 85% power and D: 100% power settings.

5.6.2 Velocity Contours

Figures 5.2A to 5.2D show velocity profiles at dividing plane of the simulated geometry (figure 4.3). In different sections of the combustion chamber, velocity slightly increases with increase in power. This is mainly because of increase in engine mass flow rate with increases in power. So the burning time in chamber would be lesser in higher power settings. However it is imperative to mention that, inlet temperatures are higher in higher power settings cases and enhances combustion by increasing kinetic rate.

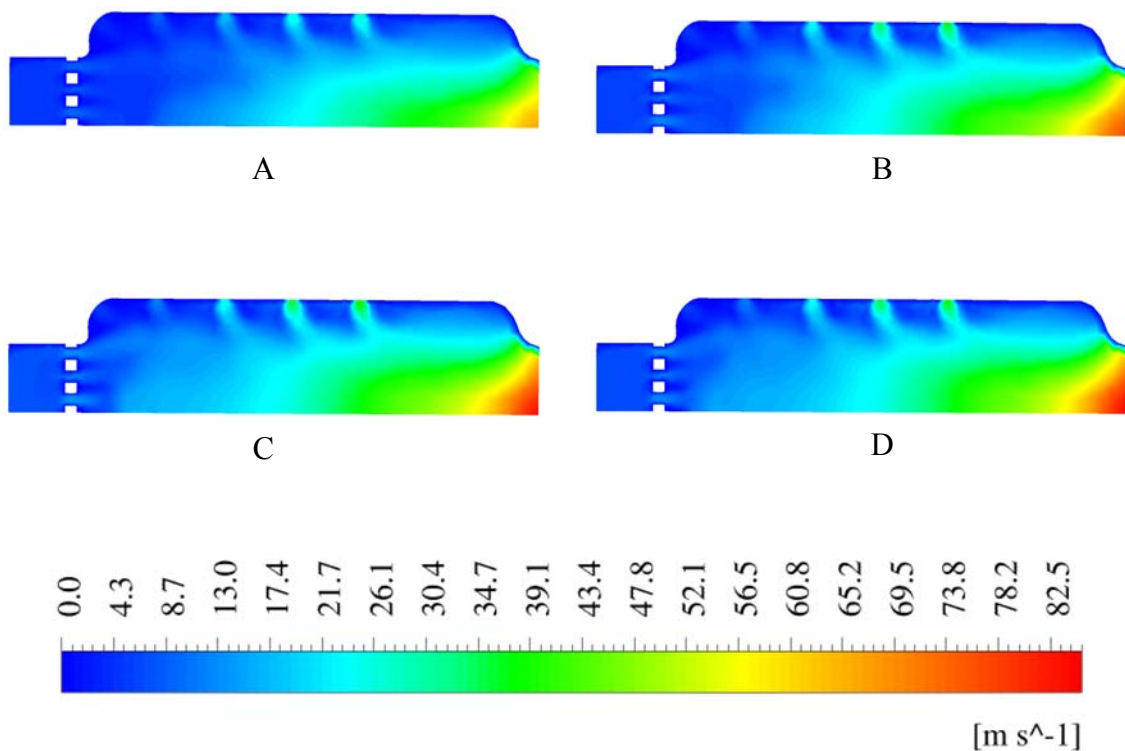


Figure 5.2 Velocity profile. A: 7% power, B: 30% power, C: 85% power and D: 100% power settings.

5.6.3 CO Mass Fraction Contours

Figures 5.3A to 5.3D, show CO mass fraction distribution (contours) at dividing plane of the simulated geometry. Figure 5.3C and 5.3D have relatively high CO concentration around the high temperature zone. The probable reason for higher CO formations in the higher power settings cases is that the rich burning occurs near high-temperature zone because 'primary-inlet' equivalence ratios in 85% is 1.4 and in 100% power settings it is 1.7 (Table 4.5). Although, this rich burning produces some CO, it helps in reducing NO_x emission by lowering the rate of NO_x formation in those zones.

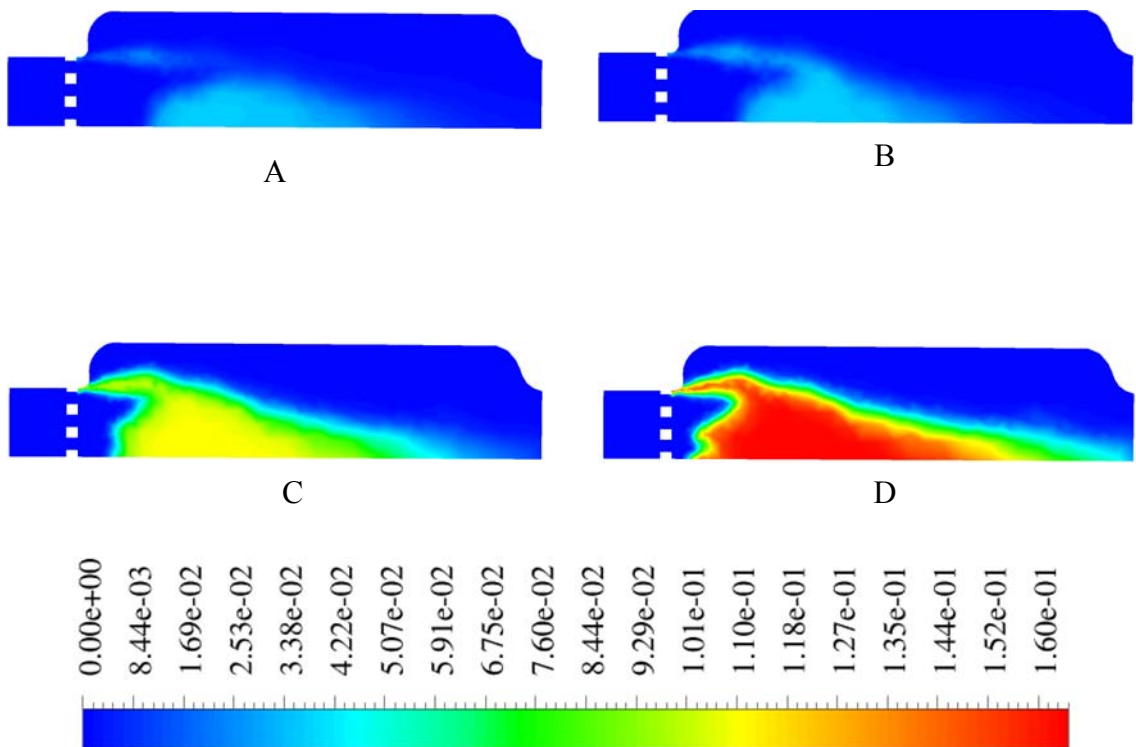


Figure 5.3 CO mass fraction. A: 7% power, B: 30% power, C: 85% power and D: 100% power settings.

5.6.4 NO Mass Fraction Contours

Figures 5.4A to 5.4D show NO mass fraction distribution at the dividing plane of the simulated geometry. For all the four cases (figure 5.4A to 5.4D), the NOx distribution is uniform. There are no high concentration NOx spots except a small region near neck of the burner for 85% (figure 5.4C) and 100% (figure 5.4D) engine power settings. Figure 5.4B shows relatively high NOx concentration than the other three cases. That is also clear from table 5.1 where NOx emission rate is the highest for 30% power setting.

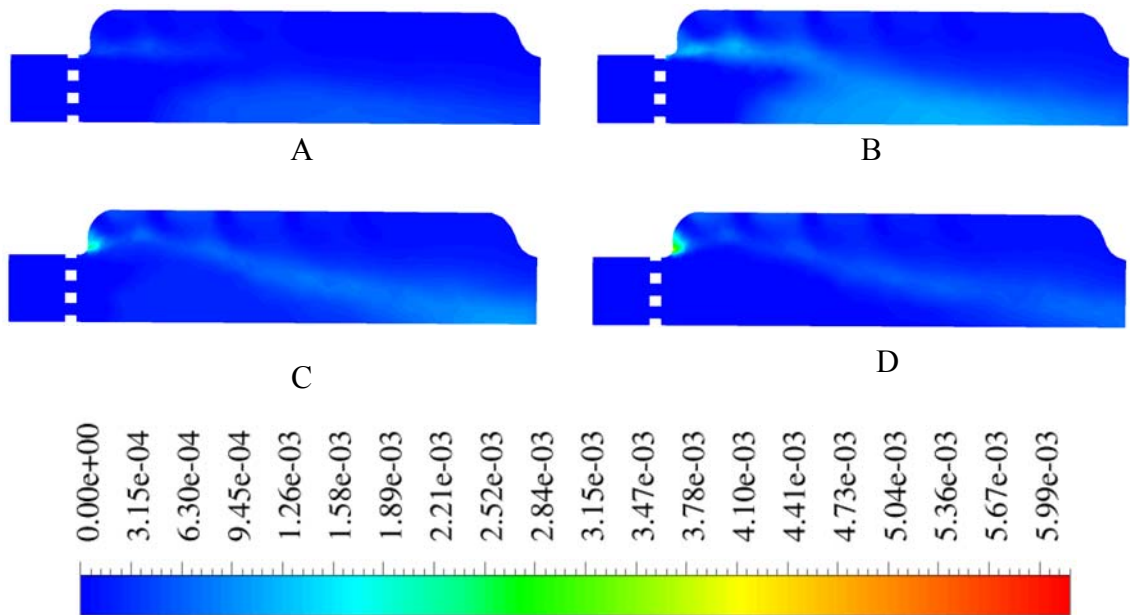


Figure 5.4 NO mass fraction. A: 7% power, B: 30% power, C: 85% power and D: 100% power settings.

5.6.5 Direction of Fluid Flow

Figures 5.5A to 5.5D, show velocity vector/directions of the fluid flow. In these figures contours have been colored by velocity magnitude. Small vectors in these figures suggest average flow direction in different region of the combustion chamber. With the increase in engine power, intensity of these vectors increases and suggests higher mass flow rate. Penetration in radial directions due to flow coming from holes is also visible from these stream-lines of vectors.

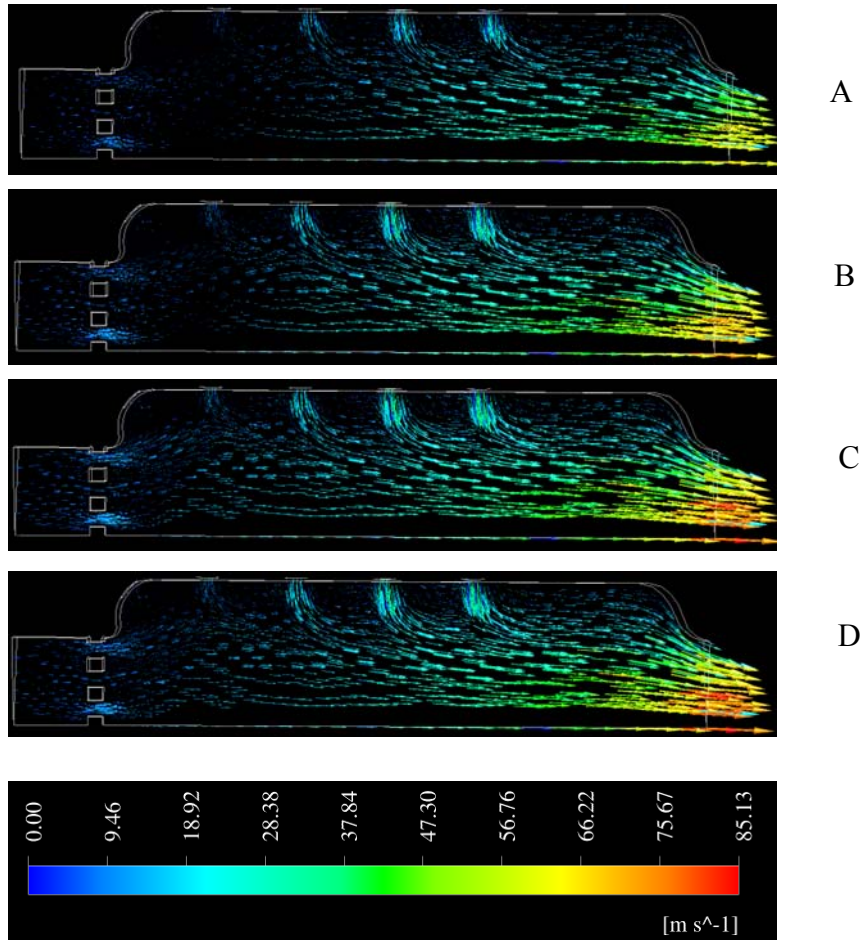


Figure 5.5 Direction of fluid flow. A: 7% power, B: 30% power, C: 85% power and D: 100% power settings.

5.7 Computational Expenses

The immense computational effort is inevitable for such modeling. As it has already been mentioned that increases in number of species affects the computational time nonlinearly. Computational time variation due to number of species variation, approximately, can be expressed as proportional to n^b , where n is number of species and b is between 2 and 3. Whereas CPU time increases proportionally with number of cell in the computational domain. Based on these assumptions the extrapolated time required to converge a simulation with our current computational facility (i.e. 2.26GHz Quad processor) for the following conditions can be calculated as follows:

Conditions:

- ✓ FLUENT (version 13) is working in its Full capacity (i.e. running a simulation with 50 species)
- ✓ A properly designed and gridded geometry (i.e. 1.1 million cell, based on [10]) will be used.
- ✓ Iterations required to converge the simulation will depend on how fast the solution is propagating toward the outlet of the combustion chamber. Solution propagation would depend on the mesh density in the axial directions. We assume it will take approximately 7550 iterations to converge such simulations.

Based on these assumptions extrapolated computational time required with the current facility can be found as follows

$$\frac{7550}{2400} \times \frac{1.1 \times 10^{+06}}{14 \times 10^{+03}} \times \left(\frac{50}{17} \right)^{2.5} \times 5hr = 18,334.7hr$$

However if we can use a super computing facility with 512 processors than number of CPU hrs would require 5.9 hr.

This simple calculation illustrates the computational effort require to solve such a combustion problem. However actual scenario may get even more complicated when discrete phase injection modeling is required in case of liquid fuel burning. Complexity will increase if there is a need to use more than 50 species.

CHAPTER 6

CONCLUSION AND RECOMMENDATIONS

A 3D CFD simulation of aircraft engine combustion process has been done. Major pollutants NO_x emission has been predicted in a fairly consistent way. Other minor pollutants species such as CO, N₂O, CH, C₂H₂ etc. have also been predicted, although there were few mismatches between the simulation results and experimental results. Among the various reasons for these mismatches, the followings can be considered as highly important.

- ✓ Faulty or inadequate kinetic scheme: The kinetic scheme [14] used in CFD simulation has been developed at 5 atmospheric pressure. But our simulations were at different operating pressure extending from nearly 3atm to 19 atm. In addition, that scheme is developed mainly for NO_x prediction, so probably; it is not a good practice to model other pollutants using that scheme. Most importantly this 17 species mechanism is not comprehensive enough to consider all the significant reaction steps and thus producing irrelevant results.
- ✓ Fuel injection system: In a real aircraft engine, complicated modern fuel injection is used to inject initial air fuel mixture. But in our case we could not afford such complicated design due to limited computational facilities.
- ✓ Air fuel ratios must be maintained in optimized conditions throughout the different burning zones. For that purpose a through sensitivity analysis needs to

be done to understand the facts associated with secondary and dilution air flow rates through different holes.

In predicting aircraft pollutants, it is highly imperative to capture the combustion process. In order to do that, we must use a detail comprehensive kinetic scheme. But such scheme is not affordable by the current computation facility. In that circumstance, reactor network model can be used with CFD calculation.

Another important fact associated with such modeling for aircraft engine emission prediction is that the experimental verification must follow these modeling, or proper co-planning must be done. Because it is not the practice, due to patent protections, to share design information either from commercial or small scale laboratory development aircraft engine, the step of experimental verification necessitates development of own experimental facility or proper collaborations with other experimentalists of same interest. Only then the model can be verified.

BIBLIOGRAPHY

1. Benini, E., Pandolfo, S., Zoppellari, S.: Reduction of NO emissions in a turbojet combustor by direct water/steam injection: Numerical and experimental assessment. *Applied Thermal Engineering* 29, 3506–3510 (2009)
2. Dooley, S., Won, S., Chaos, M., Heyne, J., Ju, Y., Dryer, F.: A jet fuel surrogate formulated by real fuel properties. *Combustion and Flame* 157, 2333–2339 (2010)
3. Dagaut, P., Bakali, A., Ristori, A.: The combustion of kerosene: Experimental results and kinetic modelling using 1- to 3-component surrogate model fuels. *Fuel* 85, 944–956 (2006)
4. Lu, T., Law, C.: Toward accommodating realistic fuel chemistry in large-scale computations. *Progress in Energy and Combustion Science* 35, 192–215 (2009)
5. Moniruzzaman, C., Yu, F.: A 0D aircraft engine emission model with detailed chemistry and soot microphysics. *Combustion and Flame* , doi:10.1016/j.combustflame.2011.11.006 (2011)
6. Fichet, V., Kanniche, M., Plion, P., Gicquel, O.: A reactor network model for predicting NO_x emissions in gas turbines. *Fuel* 89 , 2202–2210 (2010)
7. Wey, C. C., Anderson, B., Hudgins, C., Wey, C.: Aircraft Particle Emissions eXperiment (APEX). NASA/TM—2006-214382, ARL-TR-3903
8. CFM56 engine, Engine manufacturer data sheet, Accessed in December 2011. Available at: <http://www.cfm56.com>
9. Smith, R.: Advanced Low Emissions Subsonic Combustor Study. NASA/CR—1998-207931, PWA-6420-28
10. Turner, M., Norris, A., Veres, J.: High-Fidelity Three-Dimensional Simulation of the GE90. NASA/TM—2004-212981, AIAA-2003-3996
11. Benini, E., Giacometti, S.: Design, manufacturing and operation of a small turbojet-engine for research purposes. *Applied Energy* 84, 1102–1116 (2007)

12. EPA, United States Environmental Protection Agency, Accessed in May 2012. Available at: <http://www.epa.gov/air/nitrogenoxides/>
13. Hoekman, S., Robbins, C.: Review of the effects of biodiesel on NO_x emissions. *Fuel Processing Technology* 96, 237–249 (2012)
14. Kundu, K., Penko, P., Yang, S.: Simplified Jet-A/Air Combustion Mechanisms for Calculation of NO_x Emissions. In : AIAA 98-3986 (1998)
15. Lughofer, E., Macián, V., Guardiola, C., Klement, E.: Identifying static and dynamic prediction models for NO_x emissions with evolving fuzzy systems. *Applied Soft Computing* 11, 2487–2500 (2011)
16. Jiménez-Espadafor, F., M., Velez, J., Carvajal, E., Becerra, J.: Experimental analysis of low temperature combustion mode with diesel and biodiesel fuels: A method for reducing NO_x and soot emissions. *Fuel Processing Technology* doi:10.1016/j.fuproc.2011.11.014 (2011)
17. Aithal, S.: Modeling of NO_x formation in diesel engines using finite-rate chemical kinetics. *Applied Energy* 87, 2256–2265 (2010)
18. Khoshhal, A., Rahimi, M., Alsairafi, A.: CFD study on influence of fuel temperature on NO_x emission in a HiTAC furnace. *International Communications in Heat and Mass Transfer* 38, 1421-1427 (2011)
19. Schaub, G., Unruh, D., Wang, J., Turek, T.: Kinetic analysis of selective catalytic NO_x reduction (SCR) in a catalytic filter. *Chemical Engineering and Processing* 42, 365-371 (2003)
20. Mazaheri, M., Johnson, G., Morawska, L.: An inventory of particle and gaseous emissions from large aircraft thrust engine operations at an airport. *Atmospheric Environment* 45, 3500-3507 (2011)
21. Kurniawan, J., Khardi, S.: Comparison of methodologies estimating emissions of aircraft pollutants, environmental impact assessment around airports. *Environmental Impact Assessment Review* 31, 240–252 (2011)
22. Pitz, W., Mueller, C.: Recent progress in the development of diesel surrogate fuels. *Progress in Energy and Combustion Science* 37, 330-350 (2011)

23. Elliott, L., Ingham, D., Kyne, A., Mera, N.: A novel approach to mechanism reduction optimization for an aviation fuel/air reaction mechanism using a genetic algorithm. *Journal of Engineering for Gas Turbines and Power* 128, 255-263 (2006)
24. Mosbach, S., Su, H., Kraft, M.: A new algorithm for the direct simulation of combustion systems and its application to reaction elimination. *Proceedings of the Combustion Institute* 30 , 1301–1308 (2005)
25. Polifke, W., Geng, W., Dobbeling, K.: Optimization of Rate Coefficients for Simplified Reaction Mechanisms with Genetic Algorithms. *Combustion and Flame* 113, 119-135 (1998)
26. Hernández, J., Ballesteros, R., Sanz-Argent, J.: Reduction of kinetic mechanisms for fuel oxidation through genetic algorithms. *Mathematical and Computer Modelling* 52, 1185-1193 (2010)
27. Violi, A., Yan, S., Eddings, E., Granata, S.: Experimental Formulation and Kinetic model for JP-8 surrogate mixtures. *Combustion Science and Technology* 174(11&12), 399-417 (2002)
28. Humer, S., Frassoldati, A., Granata, S., Faravelli, T., Ranzi, E.: Experimental and kinetic modeling study of combustion of JP-8, its surrogates and reference components in laminar nonpremixed flows. *Proceedings of the Combustion Institute* 31, 393–400 (2007)
29. Aksit, I. M., Moss, J. B.: Model fuels to reproduce the sooting behaviour of aviation kerosene. *Fuel* 84 , 239–245 (2005)
30. Wang, T.-S.: Thermophysics characterization of kerosene combustion. *Journal of Thermophys Heat Transfer* 15 , 140–147 (2001)
31. Gueret, C., Cathonnet, M., Bottner, J.-C., Gaillard, F.: Experimental Study and Modeling of Kerosene Oxidation in a Jet Stirred Flow Reactor. *Twenty-Third International Symposium on Combustion/ The Combustion Institute*, 211-216 (1990)
32. Dagaut, P.: Kinetics of Jet Fuel Combustion Over Extended Condition: Experimental and Modeling. *Journal of Engineering for Gas Turbines and Power* 129, 394-403 (2007)

33. Mawid, M., Park, T., Sekar, B., Grana, C.: Development and validation of a detailed Jp-8 fuel chemistry mechanism. In : 38th AIAA/ASME/SAE/ASEE Joint Propulsion Conference & Exhibit, Indianapolis, Indiana (2002)
34. Dagaut, P., Cathonnet, M.: The ignition, oxidation, and combustion of kerosene: A review of experimental and kinetic modeling. *Progress in Energy and Combustion Science* 32, 48–92 (2006)
35. Cathonnet, M., Bale, s.-G., Chakir, A.: On the use of detailed chemical kinetics to model aeronautical combustors performances, In: Proceedings of the third European propulsion forum, EPF91, , , AAAF., ONERA Paris, p.313–331 (Novembe , 1992)
36. Dagaut, P., Reuillon, M., Boettner, J. C., Cathonnet, M.: Kerosene combustion at pressures up to 40 atm: Experimental study and detailed chemical kinetic modeling. *Proc Combust Inst* 25, 919–926 (1994)
37. Dagaut, P., Reuillon, M., Cathonnet, M., Voisin, D.: High pressure oxidation of normal decane and kerosene in dilute conditions from low to high temperature. *J Chim Phys Phys Chim Biol* 92, 47–76 (1995)
38. Cathonnet, M., Voisin, D., Etsouli, A., Sferdean, C., Reuillon, M., Boettner, J.: Kerosene combustion modelling using detailed and reduced chemical kinetic mechanisms. In : Symposium applied vehicle technology panel on gas turbine engine combustion, RTO meeting proceedings, NATO res. and tech. organisation, Neuilly sur seine, France, vol. 14
39. Riesmeir, E., Honnet, S., Peters, N.: Flamelet modeling of pollutant formation in a gas turbine combustion chamber using detailed chemistry for a kerosene model fuel. *Journal Eng Gas Turbine Power* 126, 899–905 (2004)
40. Dagaut, P.: On the kinetics of hydrocarbons oxidation from natural gas to kerosene and diesel fuel. *Phys Chem Chem Phys.*, 2079–2094 (2002)
41. Wen, Z., Yun, S., Thomson, M. J., Lightstone, M. F.: Modeling soot formation in turbulent kerosene/air jet diffusion flames. *Combust Flame* 135, 323–340 (2003)
42. Dagaut, P., Gail, S.: Chemical kinetic study of the effect of a Biofuel additive on Jet-A1 Combustion. *Journal of Physical Chemistry A.* 111, 3992-4000 (2007)

- 43 University of Leeds, NOx and SOx chemistry, Accessed in December 2011. Available at: <http://garfield.chem.elte.hu/Combustion/Combustion.html>
- 44 San Diego Mechanism, Combustion Research Group at University of California san Diego, Accessed in December 2011. Available at: <http://web.eng.ucsd.edu/mae/groups/combustion/mechanism.html>
- 45 Ansys, Inc. Fluid Dynamics Solutions, Accessed in May 2012. Available at: <http://www.ansys.com/Products/Simulation+Technology/Fluid+Dynamics>
- 46 CD-adapco, CFD and CAE Software, Accessed in May 2012. Available at: <http://www.cd-adapco.com/products/index.html>
- 47 GASP Software Info - AeroSoft, Inc. Providing Quality CFD Software and Solutions, Accessed in March 2012. Available at: <http://www.aerosft.com/software>
- 48 Cobalt Solutions, Cobalt Code, Accessed in April 2012. Available at: <http://www.cobaltcfd.com>
- 49 Metacomp Technologies, Inc. Computatinal Fluid Dynamics Software Suite. Available at: http://www.metacomptech.com/index.php?option=com_content&view=article&id=52:about-cfd&catid=5&Itemid=56
- 50 Manual: Ansys Meshing User's Guide. Release 13.0. (2010)
- 51 Manual: Ansys Fluent User's Guide. Release 13.0. (2010)
- 52 Manual: Ansys Theory Guide. Release 13.0. (2010)
- 53 Magnussen, B.: On the structure of turbulence and generalized eddy dissipation concept for chemical reaction in turbulent flow. In : Nineteeth AIAA Meeting , St Louis (1981)
- 54 Reaction Design, Chemkin CFD for FLUENT. Accessed in August 2011. Available at: <http://www.reactiondesign.com>
- 55 Manual: CHEMKIN-CFD for FLUENT Module. (2009)

56. Potter, M., Craig W, S.: Theory and problems of Thermodynamics for engineers. McGraw-Hill (1993)
57. Pilling, M.: From elementary reactions to evaluated chemical mechanisms for combustion models. Proceedings of the Combustion Institute 32, 27-44 (2009)

APPENDIX A
SOLVER ALGORITHMS

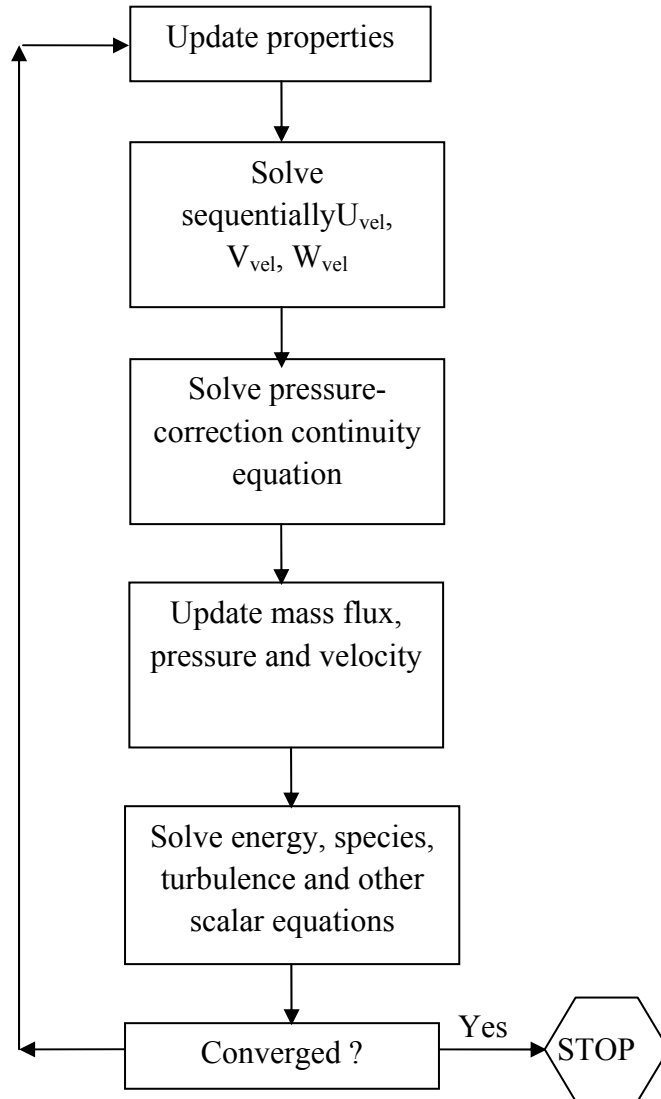


Figure A.1 Pressure Based Segregated Algorithm.

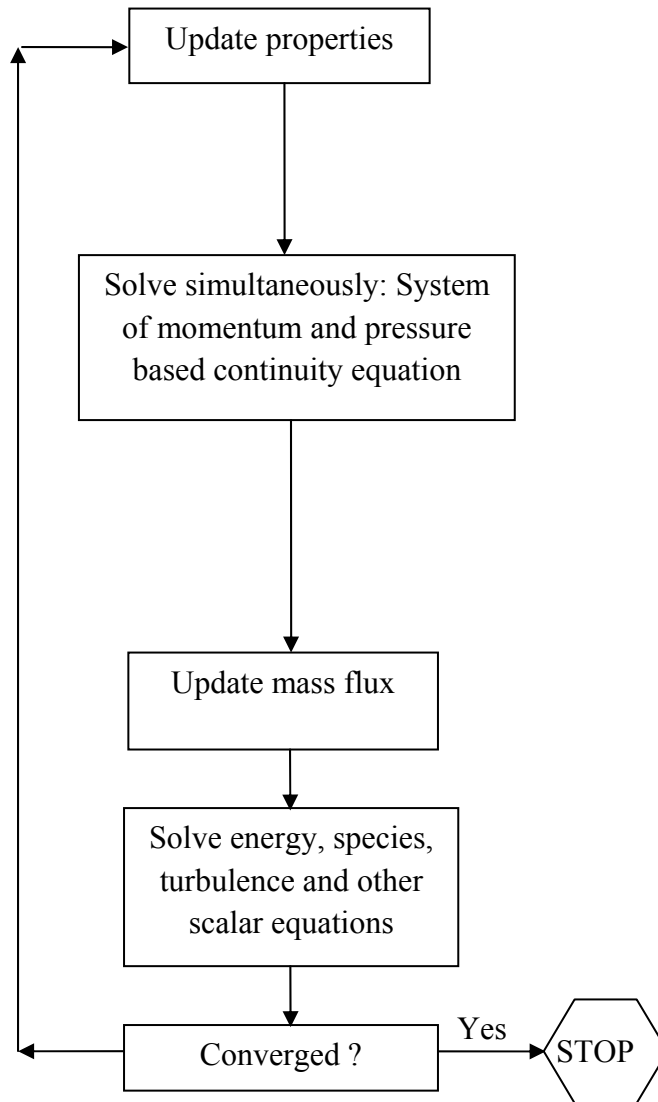


Figure A.2 Pressure Based Coupled Algorithm.

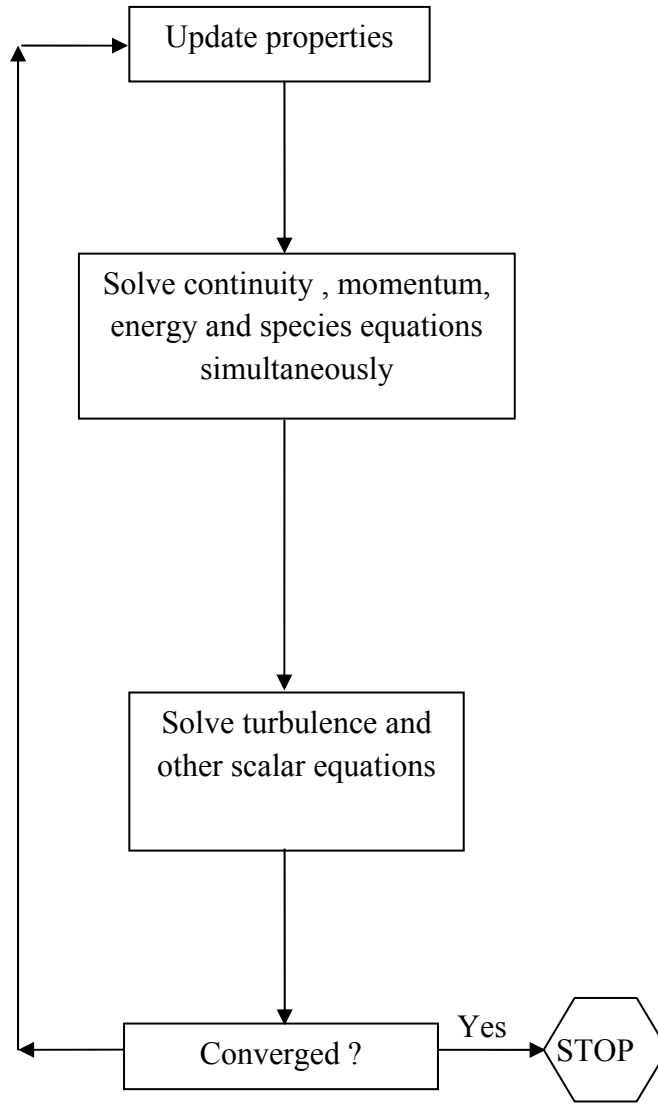


Figure A.3 Density Based Algorithm.

APPENDIX B
CHEMKIN FILES

1. CHEMKIN Format reaction mechanism file (jeta.che) used in this thesis to predict pollutants emissions. Three column after the reaction formula provide three parameters (Arrhenius factor, temperature exponent and activation energy) of Arrhenius rate expression.

```

ELEMENTS
C H O N
END
! Jet-A
SPECIES
C12H23 C2H2 CH CO CO2 O2 O OH H2 H H2O HO2 NH N NO N2O N2
END
THERMO
END
REACTIONS
! units are cm-sec-mole-cal-Kelvins.
CAL/MOLE
N2+C12H23=>12CH+11H+N2 4.35E+09 0.0 30000.0 ! 1J
FORD/N2 0.8/
FORD/C12H23 0.8/
CH+H2+N2=>2NH+CH 1.00E+15 0.0 78000.0 ! 2f
FORD/CH 1.0/
FORD/H2 0.1/
FORD/N2 1.0/
REV /1.95E+15 0.0 0.0/
CH+2NH=>N2+H2+CH 1.95E+15 0.0 0.0 ! 2b
FORD/CH 1.0/
FORD/NH 2.0/
H2+OH=H2O+H 1.17E+11 1.3 3626.0 ! 3
H2+O=H+OH 2.50E+15 0.0 6000.0 ! 4
H+O2=O+OH 4.00E+14 0.0 18000.0 ! 5
N2+O2=>2O+N2 1.00E+18 0.0 122239.0 ! 6f
H2+2O=>O2+H2 1.00E+18 0.0 0.0 ! 6b
H2+2H=2H2 2.00E+17 0.0 0.0 ! 7
H+O2=HO2 1.00E+15 -1.01 0.0 ! 8
H+HO2=H2+O2 6.50E+13 0.0 0.0 ! 9
O+HO2=OH+O2 2.50E+13 0.0 0.0 ! 10
CO+HO2=CO2+OH 5.80E+13 0.0 22934.0 ! 11
CO+OH=CO2+H 1.51E+07 1.28 -758.0 ! 12
CH+O=CO+H 3.00E+12 1.0 6000.0 ! 13
CH+OH=CO+H2 3.00E+13 0.0 0.0 ! 14
CH+NO=NH+CO 1.00E+11 0.0 0.0 ! 15

```

N2+2CH=C2H2+N2	1.00E+14	0.0	0.0	!	16
2CH=C2H2	1.00E+14	0.0	0.0		
C2H2+O2=2CO+H2	3.00E+16	0.0	19000.0	!	17
N2+O=N+NO	6.50E+13	0.0	75000.0	!	18
N+O2=NO+O	6.30E+09	1.0	6300.0	!	19
N+OH=NO+H	3.00E+11	0.0	0.0	!	20
NH+NO=N2O+H	2.00E+15	-0.8	0.0	!	21
N2O+OH=N2+HO2	3.20E+13	0.0	0.0	!	22
N2O+O=2NO	6.00E+14	0.0	28200.0	!	23
N2O+O=N2+O2	6.00E+14	0.0	28200.0	!	24
N2O+H=N2+OH	1.50E+12	0.0	0.0	!	25
NH+O=NO+H	2.50E+04	2.64	0.0	!	26
END					

2. CHEMKIN Format thermodynamic data file (therm.dat) are given below.

```
THERMO
  300.000  1000.000  5000.000
C12H23      L 6/88C  12H  23   0   OG  273.150  5000.000  1000.    1
  0.24880201E 02 0.78250048E-01-0.31550973E-04 0.57878900E-08-0.39827968E-12  2
-0.38508837E 05-0.95568240E 02 0.20869217E 01 0.13314965E 00-0.81157452E-04  3
  0.29409286E-07-0.65195213E-11-0.31310966E 05 0.25442305E 02-0.25432647E 05  4
C2H2      121386C  2H   2     G  0300.00  5000.00  1000.00  1
  0.04436770E+02 0.05376039E-01-0.01912816E-04 0.03286379E-08-0.02156709E-12  2
  0.02566766E+06-0.02800338E+02 0.02013562E+02 0.15190446E-01-0.16163189E-04  3
  0.09078992E-07-0.01912746E-10 0.02612444E+06 0.08805378E+02  4
CH      121286C  1H   1     G  0300.00  5000.00  1000.00  1
  0.02196223E+02 0.02340381E-01-0.07058201E-05 0.09007582E-09-0.03855040E-13  2
  0.07086723E+06 0.09178373E+02 0.03200202E+02 0.02072875E-01-0.05134431E-04  3
  0.05733890E-07-0.01955533E-10 0.07045259E+06 0.03331587E+02  4
CO      121286C  1O   1     G  0300.00  5000.00  1000.00  1
  0.03025078E+02 0.14426885E-02-0.05630827E-05 0.10185813E-09-0.06910951E-13  2
-0.14268350E+05 0.06108217E+02 0.03262451E+02 0.15119409E-02-0.03881755E-04  3
  0.05581944E-07-0.02474951E-10-0.14310539E+05 0.04848897E+02  4
CO2     121286C  1O   2     G  0300.00  5000.00  1000.00  1
  0.04453623E+02 0.03140168E-01-0.12784105E-05 0.02393996E-08-0.16690333E-13  2
-0.04896696E+06-0.09553959E+01 0.02275724E+02 0.09922072E-01-0.10409113E-04  3
  0.06866686E-07-0.02117280E-10-0.04837314E+06 0.10188488E+02  4
H      120186H  1     G  0300.00  5000.00  1000.00  1
  0.02500000E+02 0.00000000E+00 0.00000000E+00 0.00000000E+00 0.00000000E+00  2
  0.02547162E+06-0.04601176E+01 0.02500000E+02 0.00000000E+00 0.00000000E+00  3
  0.00000000E+00 0.00000000E+00 0.02547162E+06-0.04601176E+01  4
H2     121286H  2     G  0300.00  5000.00  1000.00  1
  0.02991423E+02 0.07000644E-02-0.05633828E-06-0.09231578E-10 0.15827519E-14  2
-0.08350340E+04-0.13551101E+01 0.03298124E+02 0.08249441E-02-0.08143015E-05  3
-0.09475434E-09 0.04134872E-11-0.10125209E+04-0.03294094E+02  4
H2O    20387H  2O   1     G  0300.00  5000.00  1000.00  1
  0.02672145E+02 0.03056293E-01-0.08730260E-05 0.12009964E-09-0.06391618E-13  2
-0.02989921E+06 0.06862817E+02 0.03386842E+02 0.03474982E-01-0.06354696E-04  3
  0.06968581E-07-0.02506588E-10-0.03020811E+06 0.02590232E+02  4
HO2    20387H  1O   2     G  0300.00  5000.00  1000.00  1
```

0.04072191E+02	0.02131296E-01	-0.05308145E-05	0.06112269E-09	-0.02841164E-13	2
-0.15797270E+03	0.03476029E+02	0.02979963E+02	0.04996697E-01	-0.03790997E-04	3
0.02354192E-07	-0.08089024E-11	0.01762273E+04	0.09222724E+02		4
N	120186N	1	G	0300.00 5000.00 1000.00	1
0.02450268E+02	0.10661458E-03	-0.07465337E-06	0.01879652E-09	-0.10259839E-14	2
0.05611604E+06	0.04448758E+02	0.02503071E+02	-0.02180018E-03	0.05420529E-06	3
-0.05647560E-09	0.02099904E-12	0.05609890E+06	0.04167566E+02		4
N2	121286N	2	G	0300.00 5000.00 1000.00	1
0.02926640E+02	0.14879768E-02	-0.05684760E-05	0.10097038E-09	-0.06753351E-13	2
-0.09227977E+04	0.05980528E+02	0.03298677E+02	0.14082404E-02	-0.03963222E-04	3
0.05641515E-07	-0.02444854E-10	-0.10208999E+04	0.03950372E+02		4
N2O	121286N	2O 1	G	0300.00 5000.00 1000.00	1
0.04718977E+02	0.02873713E-01	-0.11974958E-05	0.02250551E-08	-0.15753370E-13	2
0.08165811E+05	-0.16572504E+01	0.02543057E+02	0.09492193E-01	-0.09792775E-04	3
0.06263844E-07	-0.01901825E-10	0.08765100E+05	0.09511222E+02		4
NH	31387H	1N 1	G	0300.00 5000.00 1000.00	1
0.02760249E+02	0.13753463E-02	-0.04451914E-05	0.07692791E-09	-0.05017592E-13	2
0.04207828E+06	0.05857199E+02	0.03339758E+02	0.12530086E-02	-0.03491645E-04	3
0.04218812E-07	-0.15576179E-11	0.04185047E+06	0.02507180E+02		4
NO	121286N	1O 1	G	0300.00 5000.00 1000.00	1
0.03245435E+02	0.12691383E-02	-0.05015890E-05	0.09169283E-09	-0.06275419E-13	2
0.09800840E+05	0.06417293E+02	0.03376541E+02	0.12530634E-02	-0.03302750E-04	3
0.05217810E-07	-0.02446262E-10	0.09817961E+05	0.05829590E+02		4
O	120186O	1	G	0300.00 5000.00 1000.00	1
0.02542059E+02	-0.02755061E-03	-0.03102803E-07	0.04551067E-10	-0.04368051E-14	2
0.02923080E+06	0.04920308E+02	0.02946428E+02	-0.16381665E-02	0.02421031E-04	3
-0.16028431E-08	0.03890696E-11	0.02914764E+06	0.02963995E+02		4
O2	121386O	2	G	0300.00 5000.00 1000.00	1
0.03697578E+02	0.06135197E-02	-0.12588420E-06	0.01775281E-09	-0.11364354E-14	2
-0.12339301E+04	0.03189165E+02	0.03212936E+02	0.11274864E-02	-0.05756150E-05	3
0.13138773E-08	-0.08768554E-11	-0.10052490E+04	0.06034737E+02		4
OH	121286O	1H 1	G	0300.00 5000.00 1000.00	1
0.02882730E+02	0.10139743E-02	-0.02276877E-05	0.02174683E-09	-0.05126305E-14	2
0.03886888E+05	0.05595712E+02	0.03637266E+02	0.01850910E-02	-0.16761646E-05	3
0.02387202E-07	-0.08431442E-11	0.03606781E+05	0.13588605E+01		4
END					

3. CHEMKIN Format Transport data file (TRANSPORT.DB) are given below.

C2H2	1	209.000	4.100	0.000	0.000	2.500
C12H23	2	500.000	6.000	0.0	0.0	1.000
CH	1	80.000	2.750	0.000	0.000	0.000
CO	1	98.100	3.650	0.000	1.950	1.800
CO2	1	244.000	3.763	0.000	2.650	2.100
H2	1	38.000	2.920	0.000	0.790	280.000
H2O	2	572.400	2.605	1.844	0.000	4.000
HO2	2	107.400	3.458	0.000	0.000	1.000
N	0	71.400	3.298	0.000	0.000	0.000
N2	1	97.530	3.621	0.000	1.760	4.000
N2O	1	232.400	3.828	0.000	0.000	1.000
NH	1	80.000	2.650	0.000	0.000	4.000
NO	1	97.530	3.621	0.000	1.760	4.000
O	0	80.000	2.750	0.000	0.000	0.000
O2	1	107.400	3.458	0.000	1.600	3.800
OH	1	80.000	2.750	0.000	0.000	0.000
H	0	145.000	2.050	0.000	0.000	0.000

These data are publically available at [54]. Three files –‘jeta.che’, ‘therm.dat’ and ‘TRANSPORT.DB’ are imported into fluent pre-processor to start Chemkin solver.

Figure B.1 shows the importing process.

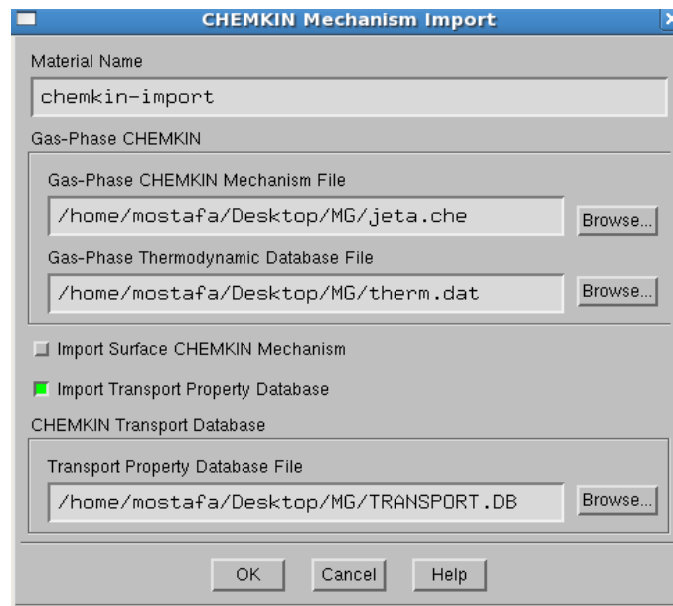


Figure B.1 CHEMKIN import in FLUENT Set-up.

APPENDIX C

MONITORING CONVERGENCE

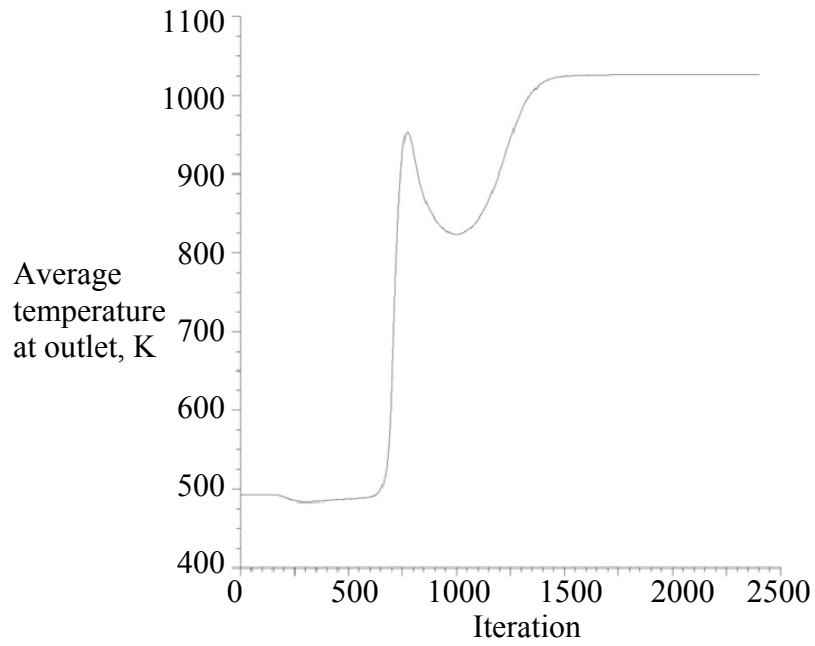


Figure C.1 Surface monitor-average static temperatures at outlet (7% power).

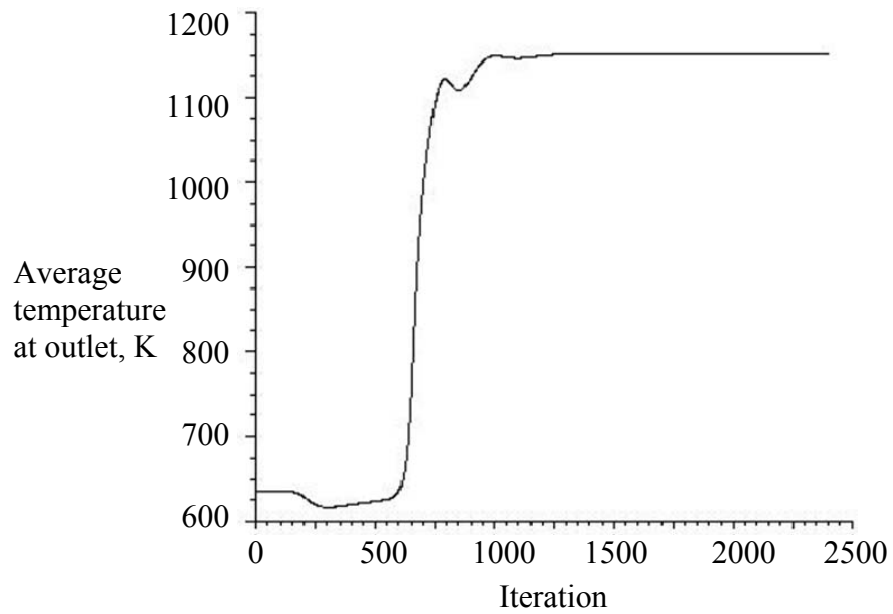


Figure C.2 Surface monitor-average static temperatures at outlet (30% power).

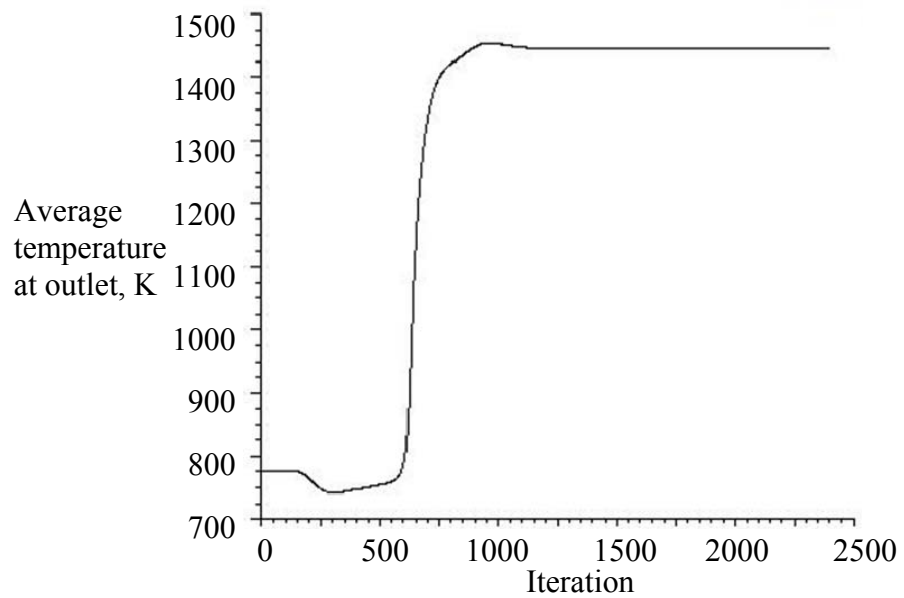


Figure C.3 Surface monitor-average static temperatures at outlet (85% power).

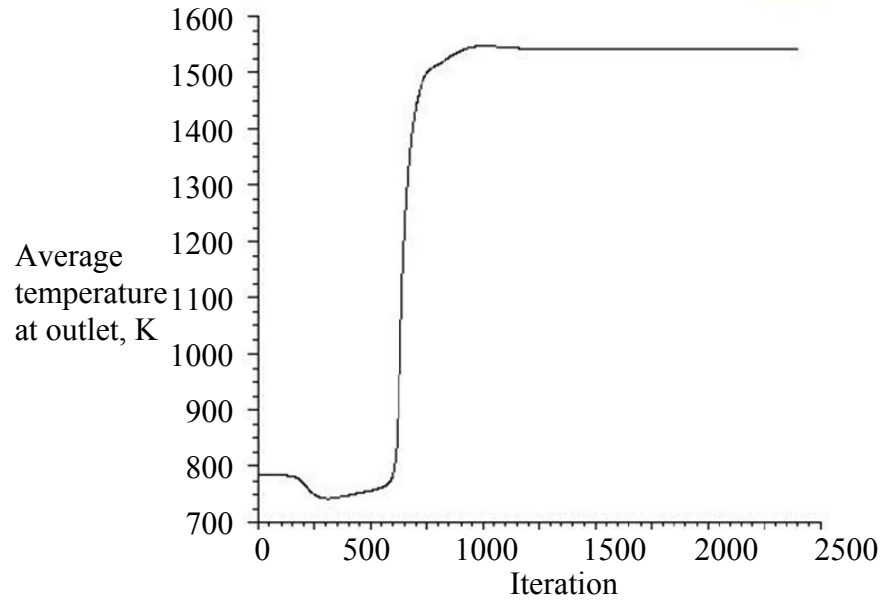


Figure C.4 Surface monitor-average static temperatures at outlet (100% power).

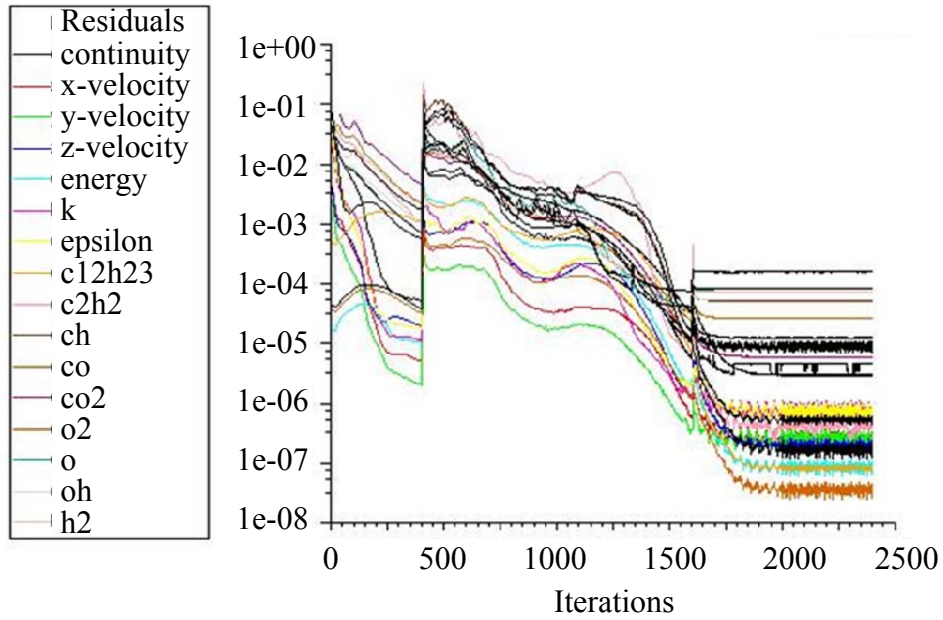


Figure C.5 Residuals -7% power settings.

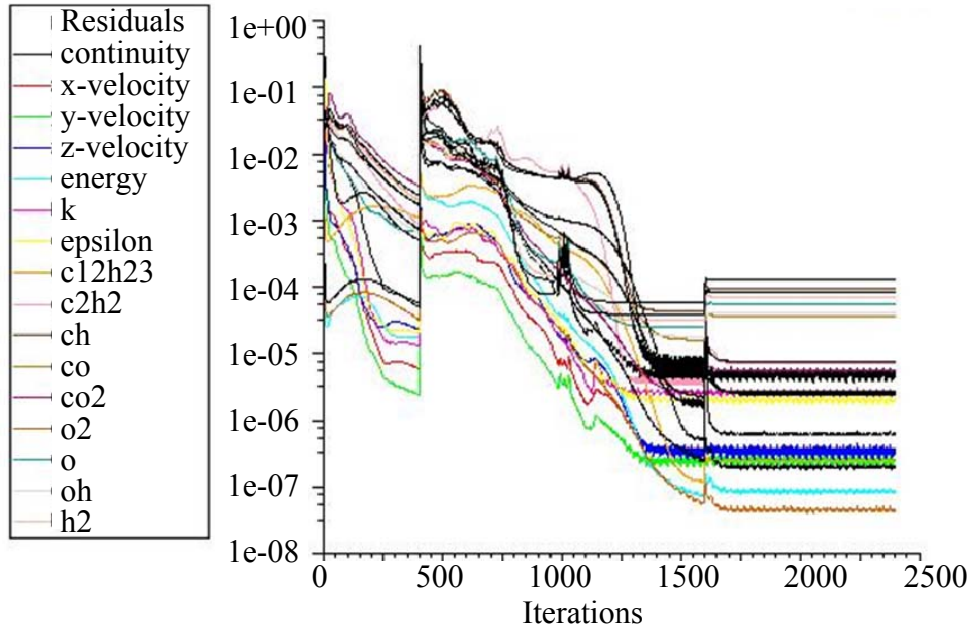


Figure C.6 Residuals -100% power settings.

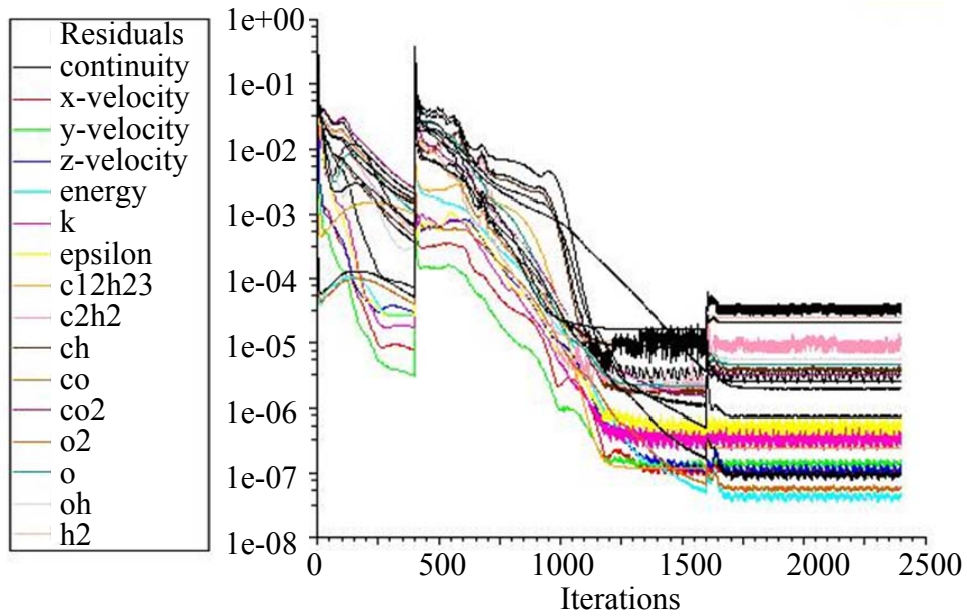


Figure C.7 Residuals -85% power settings.

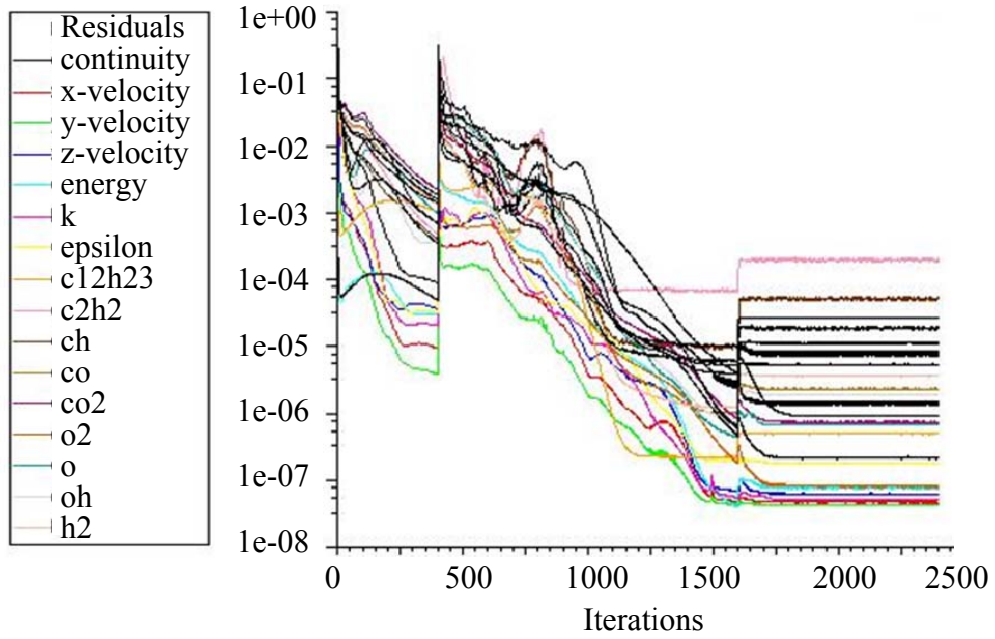


Figure C.8 Residuals -100% power settings.

APPENDIX D

ADDITIONAL CONTOUR PLOTS

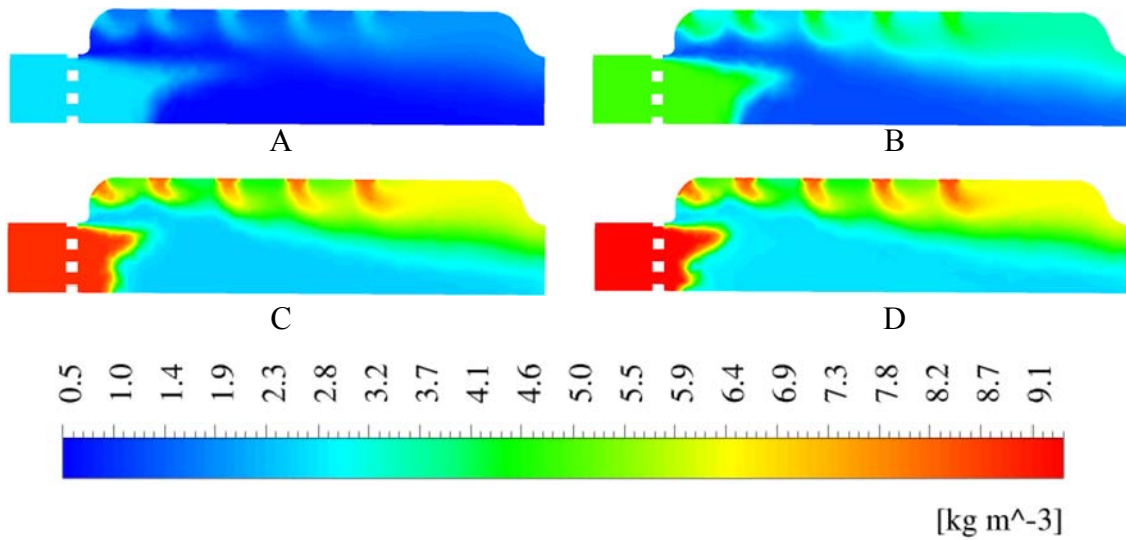


Figure D.1 Density profile. A: 7% power, B: 30% power, C: 85% power and D: 100% power settings.

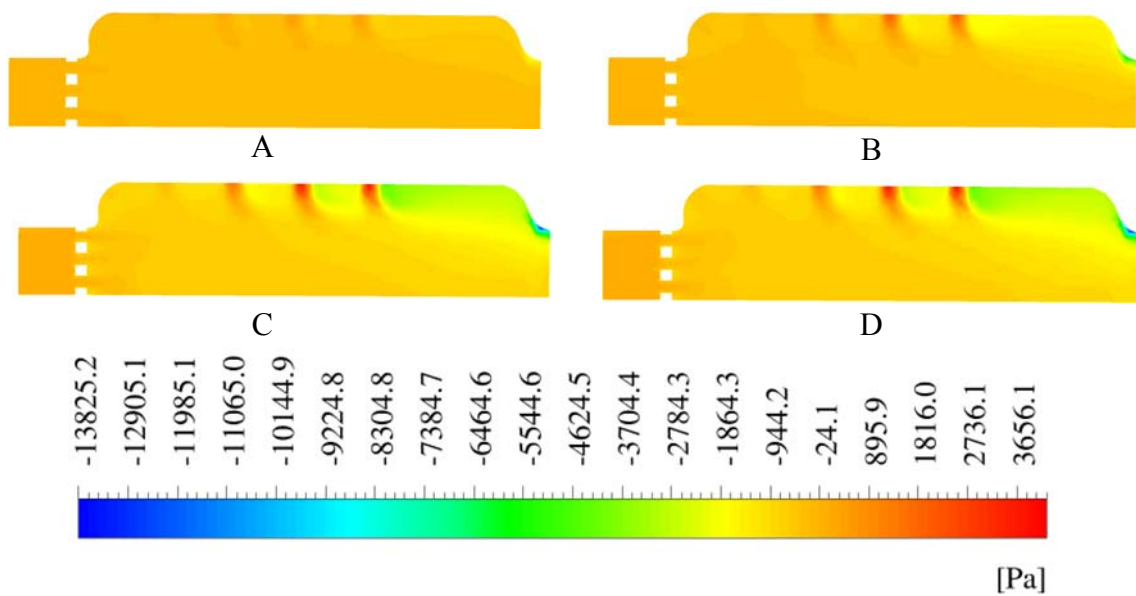


Figure D.2 Total Pressure profile. A: 7% power, B: 30% power, C: 85% power and D: 100% power settings.

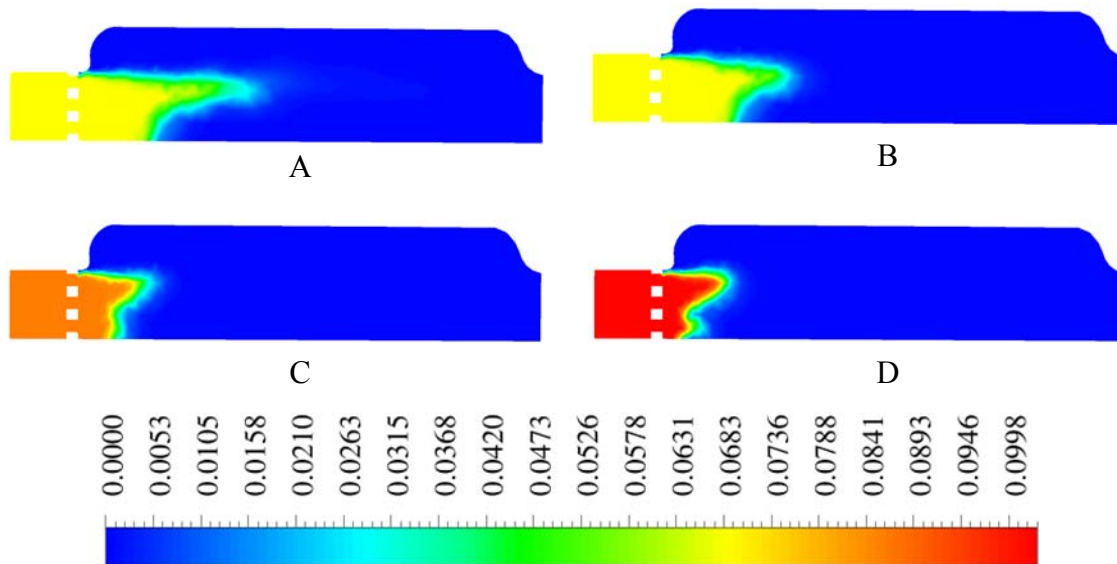


Figure D.3 Contour of $C_{12}H_{23}$ mass fraction. A: 7% power, B: 30% power, C: 85% power and D: 100% power settings.

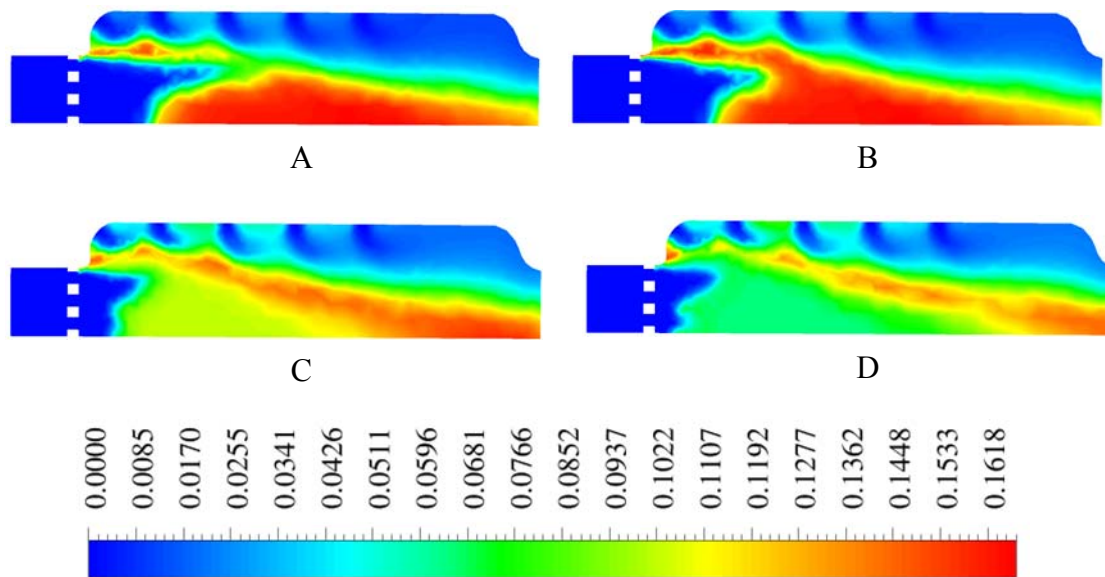


Figure D.4 Contour of CO_2 mass fraction. . A: 7% power, B: 30% power, C: 85% power and D: 100% power settings.

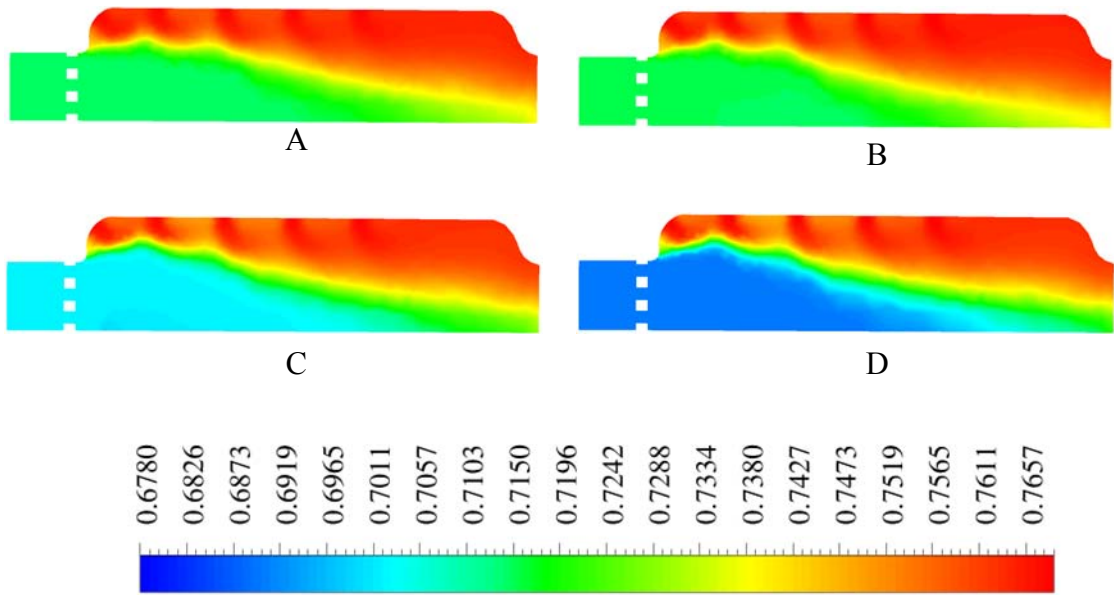


Figure D.5 Contour of N2 mass fraction. A: 7% power, B: 30% power, C: 85% power and D: 100% power settings.